IEEE Access
Multidisciplinary | Rapid Review | Open Access Journal

IEEE GEOSCIENCE AND REMOTE SENSING SOCIETY SECTION

Received 16 March 2024, accepted 28 March 2024, date of publication 1 April 2024, date of current version 5 April 2024.

Digital Object Identifier 10.1109/ACCESS.2024.3383810

RESEARCH ARTICLE

A Novel Cycloidal Scanning LiDAR Sensor Using Risley Prism and Optical Orthogonal Frequency-Division Multiple Access for Aerial Applications

GUNZUNG KIM[1], (Member, IEEE), IMRAN ASHRAF[2], JEONGSOOK EOM[3], AND YONGWAN PARK[2], (Member, IEEE)

[1]Institute of Information and Communication, Yeungnam University, Gyeongsan-si, Gyeongsangbuk-do 38541, Republic of Korea
[2]Department of Information and Communication Engineering, Yeungnam University, Gyeongsan-si, Gyeongsangbuk-do 38541, Republic of Korea
[3]Department of Multimedia and Communication Engineering, Yeungnam University, Gyeongsan-si, Gyeongsangbuk-do 38541, Republic of Korea

Corresponding author: Yongwan Park (ywpark@yu.ac.kr)

This work was supported by the Basic Science Research Program through the National Research Foundation of Korea (NRF) funded by the Ministry of Education under Grant NRF-2021R1A2B5B02086773, Grant NRF-2021R1A6A1A03039493, and Grant NRF-2022R1I1A1A01070998.

ABSTRACT This study proposes a novel light detection and ranging (LiDAR) sensor. The sensor integrates a variable field-of-view (FoV) function by utilizing optical orthogonal frequency-division multiple access (OOFDMA) to generate laser pulse streams and a Risley prism for steering. Using this approach, the LiDAR sensor can adjust the scanning pattern and density of the point cloud to match different sizes, distances, and distributions of objects. To ensure security against external threats, the LiDAR sensor incorporates advanced encryption standards (AES) and wavelength selection techniques. Additionally, the sensor employs various methods to achieve accurate and reliable measurements while minimizing mutual interference between laser signals. This innovative sensor has the potential to enhance the reliability and accuracy of LiDAR technology in aerial applications, thus facilitating the development of more advanced urban air mobility (UAM) sensors for diverse applications. The study evaluated a prototype LiDAR sensor that utilizes a coded laser pulse stream and OOFDMA technology for distance measurement. The LiDAR sensor incorporates three laser diodes with different wavelengths and a Risley prism for steering. The experimental results demonstrate that the proposed LiDAR sensor outperforms existing sensors in terms of accuracy and precision.

INDEX TERMS LiDAR, urban air mobility, Risley prism, optical OFDMA, DWDMA, variable field-of-view.

I. INTRODUCTION

Light detection and ranging (LiDAR) sensors were used to obtain information on the lunar surface where Apollo 15 landed in 1969 [1]. Since then, LiDAR sensors have been used for a variety of purposes. LiDAR mounted underneath the aircraft was used to obtain three-dimensional (3D) information on the ground on the path of the aircraft [2], [3], [4]. It was used to obtain weather information from the sky [5], [6], and 3D images of historical sites [7], [8]. The purposes for using LiDAR are different, but all are aimed at obtaining 3D stereoscopic images to obtain various information. LiDAR used only for limited purposes, attracted a more significant interest once adopted by Stanley of Stanford University [9], who used the LiDAR sensor and won the DARPA Grand Challenge. Subsequently, self-driving

The associate editor coordinating the review of this manuscript and approving it for publication was Stefania Bonafoni.

car research used it to accurately determine the available space to drive [10], [11], [12], [13]. All vehicles that require autonomous driving or autonomous walking functions are equipped with LiDAR as standard, and it is predicted that the urban air mobility (UAM) envisioned for personal aircraft will be the same [14], [15], [16], [17].

LiDAR is a representative vision sensor used in conjunction with cameras and radars. These three sensors have different advantages and disadvantages depending on their operating principles and characteristics [18], [19], [20], [21]. These sensors are used together to complement each other's shortcomings, but they continue to develop to maximize their advantages and complement their shortcomings. The camera is the only passive sensor among the three sensors and generates a two-dimensional (2D) image by receiving light reflected from an object without a separate signal source. Since there is no need for a separate signal source, only the receiver function can be maximized to quickly generate high-resolution images of a huge area, producing the best image among the three sensors. However, it does not have a light source, and measuring the distance from an object is impossible, so only 2D images can be generated using the camera. For 3D images, a method of calculating the distance is used to measure the difference in images generated by two or more cameras.

Radar is the only active sensor among the three sensors that uses radio frequency (RF) instead of light. RF has a huge divergence angle compared to light, so it can emit signals to a vast area at once and receive signals reflected from objects. Because the divergence angle is large, the distance at which the reflected signal is received is shortened. However, the impact of RF on the human body is shallow, so measurements can be made over long distances using a high-intensity signal source, creating a 3D image. Sometimes RF penetrates objects that cannot transmit light, so it is possible to receive signals reflected from two or three overlapping objects. RF technology has advanced so much that the receiver can distinguish between various frequencies with subtle differences, and by using channel division multiple access (CDMA)-based signal processing [22], the same frequency can also be distinguished in the receiver. The receiver must have many antennas to distinguish signals reflected from objects precisely. The antenna length is limited to 1/4 of the RF used by the radar, so the introduction of many antennas for high resolution has the disadvantage of making the receiving area too large [23].

LiDAR is another active sensor that uses a laser as a signal source, and most of its characteristics are located between the camera and the radar [24], [25]. Since there is almost no divergence of the signal source, the area to be measured can be divided very finely and measured at high resolution, but this requires transmitting and receiving a laser at every measuring point. In other words, the number of transmitters and receivers is proportional to the desired resolution. To improve resolution, scanning is often used to measure a large area by vertically arranging several transmitters and receivers and rotating or reflecting them [26], [27]. The scanning method measures one vertical line, and to measure a large area in detail, it operates by measuring one line and then rotating it; therefore, measurement time is needed in proportion to the size of the desired area. The vertically mounted laser diodes are fixed to the device and cannot be changed; thus, the vertical measurement angle cannot be changed. Due to these measurement characteristics, the field-of-view (FoV) is predetermined. In most cases, the horizontal and vertical resolution and spacing of the measured image are fixed and cannot be changed. LiDAR often uses Gaussian-shaped transmission and reception pulses to measure distance [28], [29]. When several LiDARs operate simultaneously, it is impossible to distinguish between pulses transmitted by the LiDAR itself and those transmitted by other LiDARs due to mutual interference [30], [31], [32], [33]. In multi-LiDAR or dense LiDAR environments, interference and crosstalk between neighboring sensors can degrade performance and accuracy, particularly in crowded urban areas or high-traffic scenarios. In the case of Velodyne LiDAR [27], a deployment method is presented to reduce mutual interference when operating multiple LiDARs simultaneously. The RF used in radar can be adjusted very precisely to create the desired frequency, but the laser used in LiDAR has a fixed wavelength for each diode, so it cannot make the desired wavelength. Additionally, the wavelength of a laser diode is determined by the material used, so the usable laser wavelength is very limited. Furthermore, because lasers are very harmful to the human body, the intensity of lasers that can be transmitted is regulated by law. Various attempts have been made to overcome the limitations of LiDAR [34], [35], [36], [37], [38], [39], [40], [41], but there is still no groundbreaking development due to physical limitations and challenges in optical signal processing.

The remainder of this paper is organized into four sections. Section II explains the operating characteristics of three different types of LiDAR. Section III describes the adaptation of the Risley prism for LiDAR technology. The concept of cycloidal LiDAR is presented in Section IV. It also contains a performance evaluation of cycloidal LiDAR. Section V explains the variable FoV scanning mechanism of the proposed LiDAR, and Section VI presents some practical applications of this LiDAR. Section VII discusses challenges and considerations for LiDAR. In the end, Section VIII concludes this study.

II. OPERATING CHARACTERISTICS OF LiDARs

Scanning LiDAR [26], [27], [42], flash LiDAR [43], and optical phased array (OPA) LiDAR [44] are three different types of LiDAR technologies, each with advantages and limitations [25], as described in Table 1. The choice of LiDAR sensor depends on factors such as application requirements, performance specifications, and cost considerations. Scanning LiDAR sensors emit laser pulses in a controlled manner, usually by rotating or oscillating a laser scanner to cover a wide FoV. They can generate

TABLE 1. Characteristics of representative commercial LiDARs.

Product	LiDAR type	Laser wavelength	Maximum range	Channels (layers)	Field-of-view		Angular resolution		Refresh rate	Pulse width
					Azimuth	Elevation	Azimuth	Elevation		
SICK LMS511 Pro	Scanning LiDAR	905 nm	80 m	1	190°	0°	0.167°	0°	25 Hz	3.6 ns
Velodyne HDL-64E	Scanning LiDAR	905 nm	120 m	64	0.167°	0°	0.08°	0.4°	5 Hz	10 ns
Velodyne VLS-128	Scanning LiDAR	903 nm	245 m	128	360°	40°	0.1°	0.11°	5 Hz	5 ns
ASC GSFL-4K	Flash LiDAR	1570 nm	100 m	8	45°	15°	0.45°	0.35°	25 Hz	10 ns
Quanergy S3	OPA LiDAR	905 nm	150 m	8	120°	10°	0.1°	0.1°	25 Hz	-

detailed 3D maps by scanning the environment from different angles. They can be used in various applications, including topographic mapping, urban planning, and autonomous navigation. They may take longer to collect data compared to other methods. The moving parts in scanning LiDAR sensors can introduce potential points-of-failure (PoF) and require maintenance. Flash LiDAR sensors illuminate the entire FoV simultaneously with a single pulse of laser light. They can instantly capture a scene, making them suitable for fast-moving objects or real-time applications. They typically have fewer moving parts than scanning LiDAR, which can increase reliability. They may have a limited range and resolution compared to LiDAR scanning, especially at longer distances, because of the safety of the eyes. OPA LiDAR sensors use an array of individually controllable optical elements to steer laser beams and dynamically adjust the direction and focus of the emitted light. They allow adaptive beam steering and dynamic beam shaping, enabling precise control over the emitted laser pulses. They can be scaled to accommodate different FoV requirements and achieve high spatial resolution. They require sophisticated control algorithms and accurate synchronization of optical elements, which can increase the complexity and cost of the sensor. Implementing OPA LiDAR technology requires advances in photonics and signal processing techniques. Each type of LiDAR technology has its unique capabilities, advantages, and limitations, making it suitable for specific applications and operational requirements. Our research is focused specifically on scanning LiDAR.

Scanning LiDAR sensors often face trade-offs between range and resolution [34], [35], [36], [37], [38], [39], [40], [41]. Increasing the range of the LiDAR sensor may reduce its spatial resolution, limiting the ability to capture fine details or detect small objects accurately. In contrast, enhancing the resolution may sacrifice range coverage, restricting the effective scanning distance of the LiDAR sensor. They may be susceptible to interference from external sources such as other LiDAR sensors, electromagnetic radiation, or reflective surfaces. Interference can distort measurements, introduce noise into the data, and compromise the accuracy and reliability of the scanning LiDAR sensor. They rely on moving components, such as rotating mirrors or oscillating scanners, to direct laser beams across the target area. These mechanical parts can introduce PoF, increase sensor complexity, and require regular maintenance, leading to potential reliability issues. By addressing these challenges through research, innovation, and collaboration, scanning LiDAR sensors can overcome technical limitations and expand their capabilities for a wide range of applications across diverse industries and domains.

Optical devices often use lenses to maximize or change optical characteristics [45]. One method is to use a single concave or convex lens, but overlapping multiple concave and convex lenses and adjusting the lens spacing can also be used. Methods that use a concave or convex lens make the lens symmetrical to its center, so light refracts equally in all directions. The prism lens has an asymmetric structure, so refraction occurs differently depending on the point at which light is incident. The Risley prism is a structure that allows rotation by overlapping multiple prisms, and the characteristic of light being asymmetrically refracted as it passes through the prism can be utilized in various forms [46], [47]. By adjusting the correlation between the prism slopes and the distance between prisms, light can be refracted in multiple forms, and multiple applications are possible using this procedure. A representative device is a phoropter, which uses the characteristics of Risley prisms to test multiple types of vision [48] One application is to create a huge mosaic image of a vast landscape by rotating the prism while keeping the camera body fixed and then collecting the results to change the desired shooting position [49], [50], [51]. Research on camera sensors or microscopes also captures very high-density images to create high-resolution images with high magnification [52], [53], [54]. Similarly, the Risley prism can also be used in an infrared line sensor to collect data from the line sensor and operate as an area sensor [55] There is also research on a camera that uses a Risley prism and a rotating mirror together to acquire images of invisible areas [56], [57], [58]. The equipment also processes the metal surface by applying a high-intensity laser to a Risley prism that moves while rotating [59]. Studies using Risley prisms indicate that the part that transmits and receives signals is fixed, and images are obtained in various areas with the desired detail using the characteristics of light refraction when the Risley prism is rotated or moved [2], [4], [5], [6], [7].

To improve the performance of LiDAR, it is essential to enhance characteristics such as maximum measurement

distance, FoV, resolution, and refresh rate. However, these characteristics are interrelated, so increasing one characteristic affects the other characteristics. To overcome the limitations of LiDAR, different methods that use various optical signal processing techniques based on optical communication are proposed. Such approaches can transmit and receive laser signals simultaneously; however, it is difficult to overcome the physical limitations of LiDAR. The method proposed in this study is an attempt to improve the performance of LiDAR by using optical orthogonal frequency-division multiple access (OOFDMA)-based optical signal processing techniques and Risley prisms together and by utilizing optical structures in addition to optical signal processing. Using OOFDMA-based optical signal processing techniques [60], [61], [62], [63], [64], laser signals can be transmitted and distinguished using multiple laser diodes of the same wavelength, which makes it possible to measure distances for various points at once, which is an excellent way to increase resolution and refresh rate. The Risley prism, which consists of three wedge prisms, is a great way to freely change the FoV and scanning area [65], [66], [67], [68], [69]. OOFDMA signals generated by laser diodes of various wavelengths are combined using an optical coupler and optical fiber.

When incident on a Risley prism, signals are refracted at different angles depending on the wavelength, using the characteristics of both the OOFDMA and the Risley prisms simultaneously. Additionally, suppose the combined laser signals are simultaneously incidental at the location of the Risley prism. In that case, they are refracted at different angles depending on the location, making it possible to measure more locations simultaneously. Optical CDMA (OCDMA) and OOFDMA technology can eliminate mutual interference even when multiple LiDARs operate simultaneously [37], [38], [39], [41], [64], [70], [71]. In LiDAR sensors, the challenge of multipath or mutual interference arises when laser pulses encounter obstacles that cause reflection or scattering. Conventional telecommunications systems employ various methods to optimize signal reception from multiple transmitters, inevitably leading to interference. LiDAR overcomes this by selectively receiving only its emitted pulses, utilizing them for distance measurement based on their unique characteristics. Employing coding techniques in O-CDMA or OOFDMA technologies enhances this property's resilience. Additionally, using multiple optical wavelengths for transmission helps mitigate interference effects. LiDAR can circumvent interference issues at specific wavelengths due to the multipath impacts by transmitting data across different wavelengths. Furthermore, by accurately estimating channel characteristics and compensating for a distortion induced by multipath propagation, the receiver can enhance the recovery of transmitted OOFDMA symbols. Moreover, the Risley prism can change the scanning area depending on the location and radius of the area being measured, allowing multiple LiDARs to operate simultaneously. It helps to measure the area wider, faster, and more precisely.

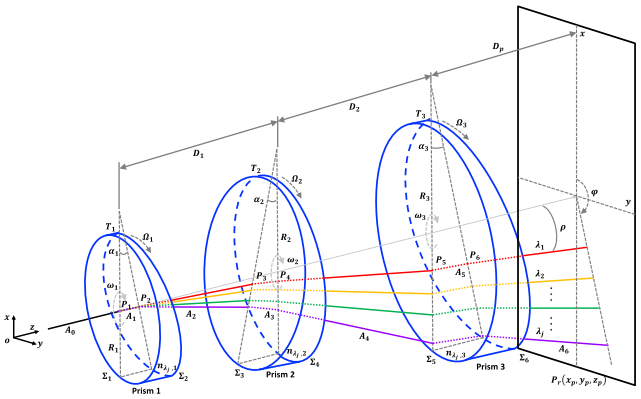

FIGURE 1. Basic configuration and coordinate system of Risley prism.

III. ADAPTATION OF RISLEY PRISM FOR TRADITIONAL LiDARs

A. BASIC OPERATION OF RISLEY PRISM

A Risley prism comprises several wedge prisms with different inclination angles and sizes [46], [47]. The laser incident on the Risley prism is refracted each time it passes through the prism, and the wavelength of the light determines the final refraction angle, the angle of incidence, the refractive index and inclination angle of the prism, and the distance between the prisms. Even if all the characteristics of the prism are the same, the refractive index varies depending on the wavelength of light, so the path along which the light travels also changes. Even if light of several wavelengths is collected and incident on a Risley prism, it is separated into several lights depending on the wavelength. When the prisms inside a Risley prism are rotated, the angle of inclination and incidence between the prisms change, thereby changing the path along which light travels. Using these characteristics of Risley prisms, it is possible to create various shapes for light to reach.

B. OPERATION OF TRADITIONAL LiDARs

LiDAR is used in many places, including self-driving cars, to detect objects in 3D [10], [11], [12], [13]. The most widely used scanning LiDARs are the Sick LMS series and the Velodyne HDL series [66], [72], [73]. Sick's LMS series is a LiDAR sensor that measures only one vertical location and changes the measurement direction using a mirror mounted inside [26], [74]. After measuring one location, rotate the internal mirror slightly to measure the next angle. Since only one point is measured vertically, the time required for measurement is proportional to the maximum measurement distance, and the refresh rate is inversely proportional to the number of angles through which the mirror is rotated. Because only one location is measured at a time, only one laser pulse is periodically sent from a laser diode fixed to the device.

Velodyne's HDL series has separate products with 16, 32, 64, and 128 vertical measurements, but the overall operating principle is the same [27], [75], [76], [77]. Each product

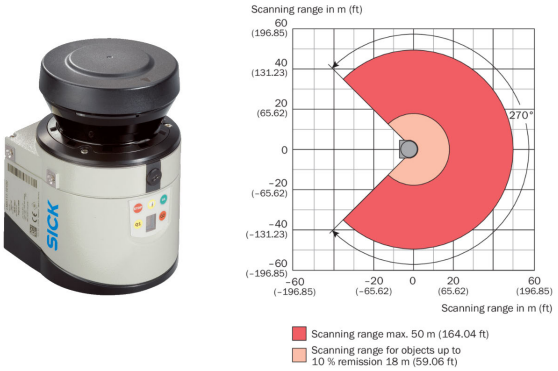

FIGURE 2. Sick LMS series LiDAR and scanning area.

(a) Veloline's 128-channel Alpha Prime

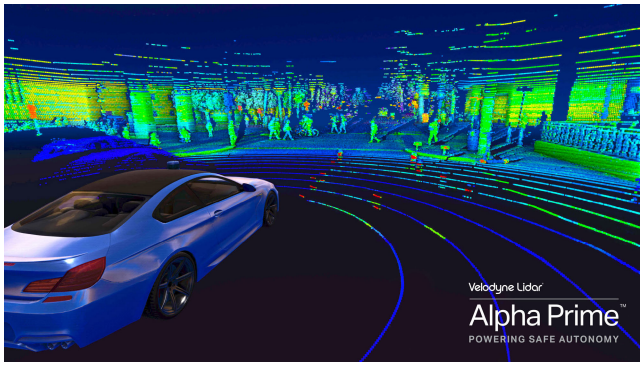

(b) Results measured with Velodyne's Alpha Prime

FIGURE 3. Velodyne's Alpha Prime series is a high-performance LiDAR that measures 128 vertical channels simultaneously. Each channel accurately measures the distance and position of surrounding objects according to a fixed angle.

has the same number of laser diodes fixed to the device as the number measured vertically. If vertically mounted laser diodes all transmit laser pulses simultaneously, even if the laser pulse reflected from the object is input to the receiver, it is tough to distinguish which laser diode transmitted the laser pulse. The vertically mounted laser diodes are divided into several blocks, and only one laser diode emits a laser from each block in a particular order to minimize mutual interference. After measuring the distance, another laser diode in the block emits a laser to measure the distance. Laser diodes in different blocks can operate simultaneously, but only one laser diode in the same block can operate at a time. After measuring the distance using all laser diodes in the block, the body rotates slightly to measure the next angle. Measuring one angle by measuring multiple points vertically requires more time than Sick's LMS series. For Velodyne's HDL series, the measurement time is proportional to the maximum measurement distance and the number of laser diodes included in the block, and the refresh rate is inversely proportional to the number of angles through which the body rotates. Velodyne's HDL series has a slow refresh rate but can measure multiple locations vertically from a single angle, making it a top-priority product for many researchers, including self-driving cars. The refresh rate is very low, which is disadvantageous when detecting fast-moving objects.

C. TRADITIONAL LiDARs WITH RISLEY PRISM

This section elaborates on what happens when a Risley prism is applied to an existing lidar. When a Risley prism is mounted on Sick's LMS series, the position where the laser pulse is transmitted from the laser diode is permanently fixed, so the position where the laser pulse is incident on the Risley prism is also always fixed [26], [46], [47], [74]. First, let us look at the case where the LMS series does not rotate, and only the Risley prism rotates. If the internal prisms of a Risley prism do not rotate, the angle at which the laser pulse is refracted is fixed. Due to the mutual relationship between the prisms inside the Risley prism, the laser pulse is always refracted and sent out in a specific direction, so the position at which the distance is measured is also constant. When a Risley prism rotates, the angle of refraction is determined by the position at which the laser pulse is incident on the Risley prism and the mutual relationship between the prisms within the Risley prism. When a laser pulse is incident on the center of a Risley prism, the laser pulse is refracted according to the unique scanning pattern created by the Risley prism, and the distance is measured in a pattern similar to the scanning pattern. The farther the incident location is from the center of the Risley prism, the more refraction occurs. The overall refractive index changes greatly depending on the correlation between the prisms inside the Risley prism, resulting in a huge change in the position where the distance is measured. In some cases, the distance is measured according to a scanning pattern different from the unique scanning pattern created by the Risley prism. When the LMS series rotates, the mirror mounted inside the lidar rotates around the z-axis in a spherical coordinate system and continuously changes the azimuth at which the laser is transmitted. The Risley prism must also rotate around the z-axis at the same angular speed as the internal mirror to maintain the angle refracted by the Risley prism. The scanning pattern of the LMS series is ultimately determined by various factors such as the rotation speed of the lidar, the rotation speed of the Risley prism, the rotation speed of the prisms inside the Risley prism, and the position at which the laser pulse enters the prism.

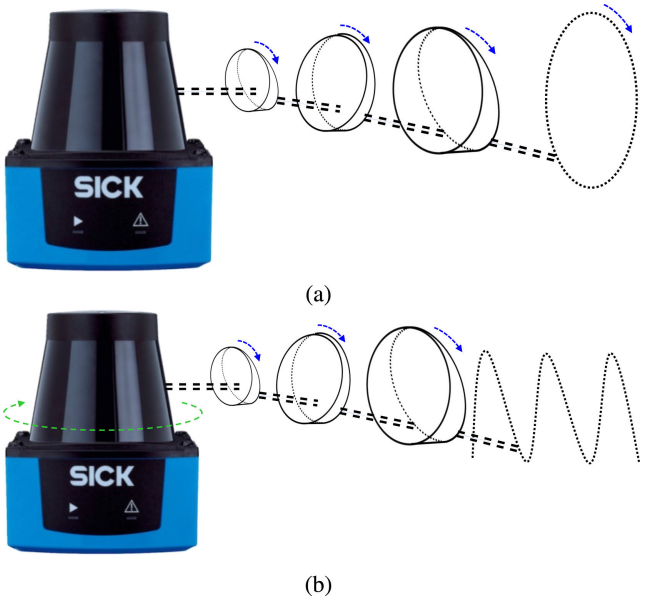

FIGURE 4. These are scanning patterns created by refracting laser pulses when a Risley prism is attached to the lidar of the Sick LMS series. Although the LiDAR's unique scanning pattern is lost, the scanning pattern is predictable depending on the LiDAR rotation speed and the rotation speed of the Risley prism. (a) A Risley prism refracted the scanning pattern while the lidar was stationary. (b) A Risley prism refracted the scanning pattern while the lidar was rotating.

Velodyne's HDL series transmits multiple laser pulses vertically, making it more difficult to predict the scanning pattern when using a Risley prism [27], [46], [47], [75], [76], [77]. In the case of the Alpha Prime model, which can measure distances in 128 directions, laser pulses are divided into several blocks, and the order in which they transmit lasers is predetermined. In addition, as shown in Figure 6, the laser diodes are not vertically arranged in a row. Still, they are widely arranged according to the unique azimuth and zenith angles specified for each laser diode. The azimuth and zenith angles between the laser diodes are all spaced differently, making it difficult to find a specific scanning pattern. Even though a Risley prism is mounted and fixed at the part where the laser is transmitted, the position at which each laser diode enters the Risley prism is different. The angle of refraction is also different. When the prisms inside a Risley prism rotate, a more significant change occurs in the refraction angle. This change occurs even more when the laser transmission interval and prism rotation speed differ. This aspect becomes more evident when the lidar rotates around the z-axis of the spherical coordinate system, and the Risley prism also rotates around the center of the prism. The scanning pattern of the HDL series also includes the azimuth and zenith angles of the laser diode, the laser transmission sequence, the rotation speed of the lidar, the rotation speed of the Risley prism, the rotation speed of the prisms inside the Risley prism, and the position at which the laser pulse enters the prism. The final decision is made based on various factors.

Existing scanning lidar products have unique rotation and laser transmission characteristics, so obtaining the desired

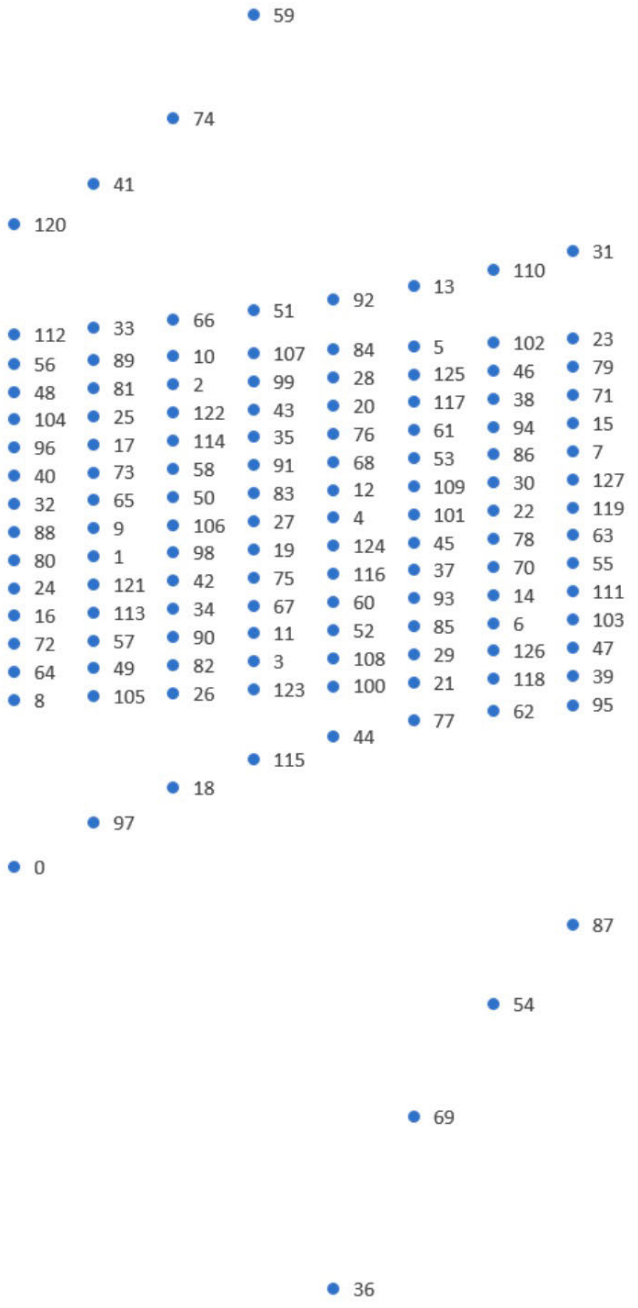

FIGURE 5. Alpha Prime is a product that measures the surrounding environment with 128 channels, and the azimuth and zenith angles are different for each channel.

scanning pattern using a Risley prism is difficult. Depending on the laser diode's laser transmission direction, the incident position of the Risley prism, and the prism correlation within the Risley prism, some laser pulses are refracted further outward than the inherent laser transmission direction, and some laser pulses are refracted further inward. In particular, Velodyne's LiDAR divides the laser diodes into several blocks to eliminate mutual interference, and the transmission order is also determined. If a Risley prism is attached, some laser pulses may be transmitted or received in a similar

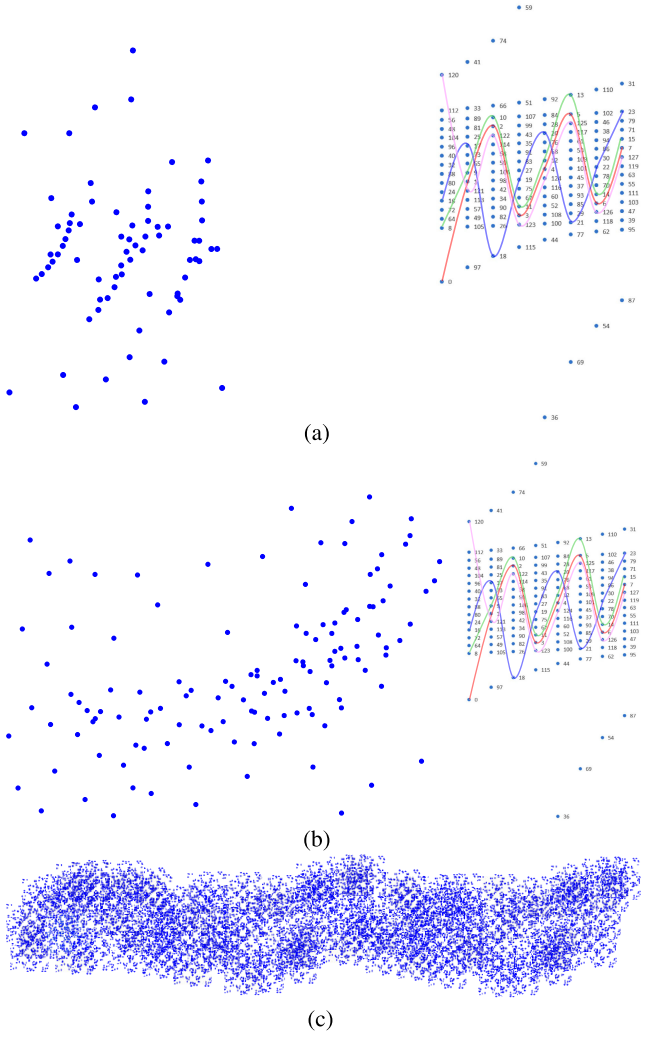

FIGURE 6. These are scanning patterns created by refracting laser pulses when a Risley prism is attached to the lidar of the Velodyne Alpha Prime. Similarly to Sick LMS, the LiDAR's unique scanning pattern is lost, and the scanning pattern is unpredictable depending on the LiDAR rotation speed and the rotation speed of the Risley prism. (a) Scanning pattern in which the laser transmitted from 128 channels is refracted by the Risley prism when Alpha Prime is stopped. (b) Scanning pattern in which the laser transmitted from 128 channels is refracted by the Risley prism when Alpha Prime rotates. (c) When Alpha Prime's laser pulses overlap, the scanning pattern is refracted by a Risley prism for a long time.

direction due to refraction caused by the Risley prism, resulting in more mutual interference. Existing LiDARs do not consider lenses when transmitting laser pulses. So, all unique measurement characteristics and advantages are lost if any optical part such as a concave lens, convex lens, or Risley prism is attached. An appropriately designed LiDAR is needed to effectively utilize the characteristics of optical sensors such as Risley prisms.

D. LiDARs WITH RISLEY PRISM

Traditional scanning lidar measures one line vertically and then slightly moves the angle to measure the following line. Because all optical components are fixed, an optimized measurement that depends on the measurement target is not possible. It is impossible to change the LiDAR's FoV or measurement direction. If it is more effective to measure the measurement object horizontally or diagonally when mounted on an autonomous vehicle, attach it to the vehicle so that it can be measured horizontally or diagonally. A single LiDAR can always measure only the FoV determined by the scanning method and the mounting location. Scanning LiDARs measure one line vertically and then change the angle at a predetermined angle, so the density decreases proportionally to the distance from the LiDAR. Areas close to the LiDAR are measured closely and sufficiently to recognize even small objects. However, distant locations are measured loosely, and in the case of small objects, there are cases where measurement is not possible at all. When multiple laser pulses with different wavelengths are incident on a prism, the refractive index is different depending on the wavelength, so the angles emitted from the prism are all different, allowing multiple angles to be measured simultaneously. The refractive index is fixed depending on the prism's medium and the laser's wavelength, but the Risley prism is composed of several wedge-shaped prisms, so the spacing between prisms can be adjusted. When the prism rotates, the thickness of the prism changes and the angle of refraction can be changed. Using a Risley prism in the LiDAR transmitter allows the optimal scanning density and pattern to be selected depending on the measurement area or target. When the central axis of the prism is moved, the measurement direction can be changed, allowing the measurable areas to be adjusted separately from the mounting position. If the rotation speeds of the prisms are the same, they are measured in a circular shape; if the rotation speeds are different, they are measured with various scanning patterns. The angle at which light is refracted can be changed by adjusting the spacing between prisms, so the prism spacing can be adjusted according to the distance to maintain the same measurement interval. By changing the scanning pattern and prism spacing that measures near and far, even small objects can be measured regardless of distance. If necessary, it is possible to collect the central axis of the prism in a specific direction and measure multiple LiDARs simultaneously. Existing LiDARs have predetermined scanning patterns, so a Risley prism can have the opposite effect. If you design a lidar optimized for the Risley prism, you can take advantage of the various characteristics of the Risley prism.

IV. CYCLOID SCANNING LiDAR USING RISLEY PRISM AND OOFDMA

Because of its ability to acquire high-resolution 3D images, LiDAR is used in many places to detect objects. Among the various types of LiDAR, scanning LiDAR, which uses laser pulses to transmit and receive, is the most widely used. Pulse-type scanning LiDARs have a trade-off relationship between performance indicators such as maximum measurement distance, FoV, resolution, and refresh rate, so when one characteristic improves, the other characteristic

deteriorates. The authors proposed LiDARs using various optical communication techniques to reduce the trade-off between pulse LiDAR characteristic indicators and proved their effectiveness through experiments and simulations [35], [38], [41], [71], [78], [79]. Although it is possible to bypass or reduce the trade-off of LiDAR characteristic indicators using various optical communication techniques, it is impossible to eliminate the physical characteristics of the laser. In this paper, we propose a LiDAR that significantly improves performance and flexibility by shortening the trade-off relationship of characteristic indicators as much as possible by using the wavelength and refraction characteristics of the optical part along with optical communication techniques.

As a next-generation LiDAR that flexibly responds to various environments, we design a scanning LiDAR with the following characteristics to make the most of the flexible optical characteristics of Risley prisms [46], [47], [65], [66], [67], [68], [69].

- Depending on the operating environment or purpose, it can be replaced with various optical parts such as Risley prisms, concave, convex, and double lenses.
- Multiple locations can be measured simultaneously using the refraction of the optical part
- While measuring rotation based on the center of the optical part, measuring rotation around the z-axis of the spherical coordinate system
- More than one LiDAR operates simultaneously to improve detection characteristics further

OOFDMA was selected as an optical signal processing technology suitable for Risley prisms. OOFDMA is one of the optical communication methods that can transmit and receive data to multiple places at the same time and has the following outstanding characteristics [60], [61], [62], [63], [64], [65], [66], [67], [68], [69], [80], [81], [82], [83], [84]. Details of the structure and behavior of LiDAR-based on OOFDMA are described in our paper [64]. We provided in-depth technical insights into the coding methods used, particularly examining the impact of OOFDMA on LiDAR performance. We explored the specific advantages of integrating DHT with PAM and how this sensor can effectively distinguish between multiple laser signals. Our analysis was supported by system architecture, operations, simulations, and experimental findings to elucidate these concepts fully. The structure, operation, and properties of the Risley prism are described in [47].

- Data can be transmitted and received from multiple locations simultaneously by adopting the orthogonal frequency division method.
- To naturally use optical characteristics that can only express 0 and 1, pulse amplitude modulation (PAM) and discrete Hartley transform (DHT) are used.
- The result of encoding the information indicating the measurement direction using OOFDMA technology is very short. Hence, the time to transmit and receive the encoded laser pulse is very short.
- It is well integrated with dense wavelength division multiple access (DWDMA), allowing simultaneous data transmission and reception using laser signals of different wavelengths.

A. BASIC OPERATING CONCEPT

This study presents a new LiDAR that utilizes OOFDMA to generate a laser pulse stream and a Risley prism for steering, as illustrated in Figure 11. The proposed LiDAR incorporates a variable FoV function that adjusts the scanning pattern and density of the point cloud to correspond to different sizes, distances, and distributions of objects. The proposed LiDAR employs multiple pulses generated by special coding techniques, rather than a single pulse, to ensure that only the pulses it emits are distinguishable, eliminating mutual interference [34], [35], [37], [38], [39], [71], [78]. However, coding techniques in optics can only use the presence of light, limiting them to represent only zeros and positives, unlike RF, which can represent negative numbers. A very long pulse stream is required to represent a single bit in opticals, which results in a long time to transmit the pulse stream [63], [79]. OOFDMA is a computationally intensive coding technique that produces very short pulse streams, which makes it suitable for LiDAR [62], [63]. The pulse streams are refracted according to the emitted laser wavelength and directed toward the target direction. This LiDAR uses pulse streams coded with OOFDMA to encode information into a very short length, which is then carried out on multiple wavelengths from DWDMA recommendations. The Risley prism is adjustable and contains multiple prisms, enabling the sensor to achieve variable FoV for distance and measurement density in a specific region of interest (ROI). By adjusting the prism angles and angular velocities, the Risley prism can have various scanning patterns and obstacle distances can be altered by changing the spacing between prisms according to the ROI, as illustrated in Fig. 1.

The proposed LiDAR maximizes the characteristics of the Risley prism by using OOFDMA and DWDMA together. All laser diode signals use OOFDMA, generating direction information as a very short laser signal. Laser diodes generate laser signals of different wavelengths specified by DWDMA. Laser signals of different wavelengths are combined into one laser signal using an optical coupler and then incident on the desired location of the Risley prism. Each time it passes through the prism inside the Risley prism, one laser signal is divided into several laser signals depending on the wavelength and the angle of incidence, inclination, and refractive index of the prism. The split laser signals are sent out in different directions, then reflected by the objects and received by the photodiodes. Photodiodes have a filter, so they only receive the wavelength of each designated laser signal, and through the OOFDMA decoding process, direction information and transmission time information are determined, and the distance and direction to the object are determined to generate a 3D image.

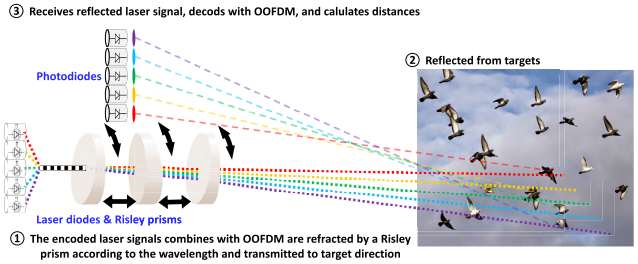

FIGURE 7. If the proposed LiDAR is mounted on a UAM, even fast-flying small birds can be detected.

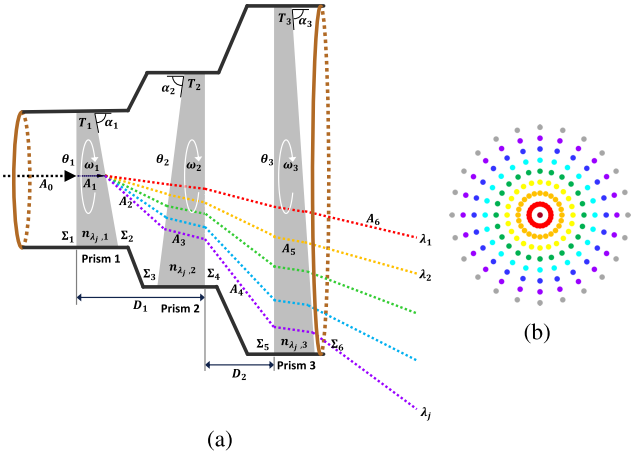

FIGURE 8. These are scanning patterns created by refracting laser pulses when a Risley prism is attached to the lidar of the Sick LMS series. Although the LiDAR's unique scanning pattern is lost, the scanning pattern is predictable depending on the LiDAR rotation speed and the rotation speed of the Risley prism. (a) Schematic diagram illustrating rotating triple Risley prism scanning model. (b) Cycloidal scanning pattern by a rotating Risley prism and OOFDMA.

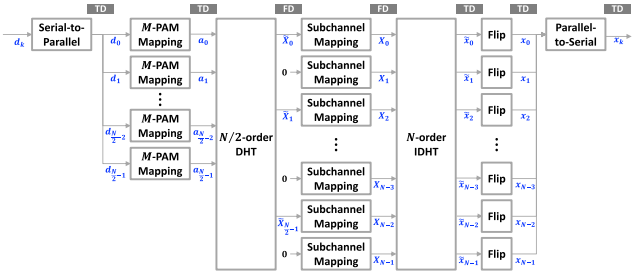

FIGURE 9. Signal processing sequences of the HTP-based flip-OFDM encoder at each transmission carrier.

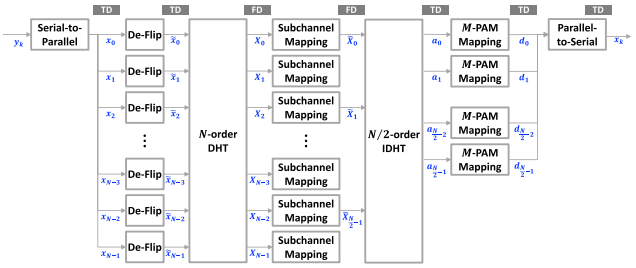

FIGURE 10. Signal processing sequences of the HTP-based flip-OFDM decoder at each receiving carrier.

The Risley prism used in the proposed LiDAR consists of three wedge prisms with different sizes and slopes. The three prisms can operate independently of each other and rotate individually, and the distance between the prisms is also adjustable. The laser incident on the exact center of the Risley prism is refracted at different angles because the refractive index varies depending on the wavelength in the first prism. Lasers incident on the second prism are refracted depending on the wavelength, and lasers incident on the third prism are also refracted depending on the wavelength. When lasers incident on the first prism at the exact location pass through all three prisms, they are emitted in different directions with different refraction angles depending on the wavelength. When the three prisms rotate, the angle of incidence continues to change depending on their relationship, which becomes the most critical factor in determining the direction of transmission. Various scanning patterns can be created by adjusting the relative rotation speeds of the three prisms.

The proposed LiDAR employs various techniques to ensure accurate and reliable measurements while minimizing mutual interference between laser signals. One of these techniques involves using the device and encrypted identifiers to specify the transmission direction of the corresponding laser signal. By modulating the encrypted identifiers through OOFDMA modulation, multiple laser signals with different wavelengths can be generated and transmitted simultaneously in various target directions. This approach prevents mutual interference between laser signals transmitted simultaneously or by other LiDARs. Additionally, LiDAR utilizes pulse streams generated by optical coding techniques to ensure that only the pulses it emits are distinguishable, thus eliminating mutual interference. However, optical coding techniques are limited in representing positive and negative numbers, unlike RF. LiDAR uses OOFDMA, a computationally intensive coding technique that produces very short pulse streams to overcome this limitation, making it well suited for LiDAR. Changing the transmission direction of the laser signal, irrespective of whether a reflected signal is received, also reduces the latency for distance measurement.

The transmission data are generated using flip-OFDM based on Hartley transform precoded (HTP) based on DHT and separated into each subchannel [60], [61], [62], [63], as shown in Figure 9 and 10. The prisms are rotated in accordance with the direction of laser pulse emission and measurement interval of LiDAR scanning. The linear movement of the prisms is controlled to ensure an appropriate measurement density [47], [85]. Once the received subchannels are combined, OOFDMA restores the data. In addition to measuring objects' distance and movement speed, the proposed LiDAR measures the time of flight (ToF), signal strength, pulse width, and Doppler frequency. Various signal processing techniques, including optical aberration correction, are utilized to enhance the

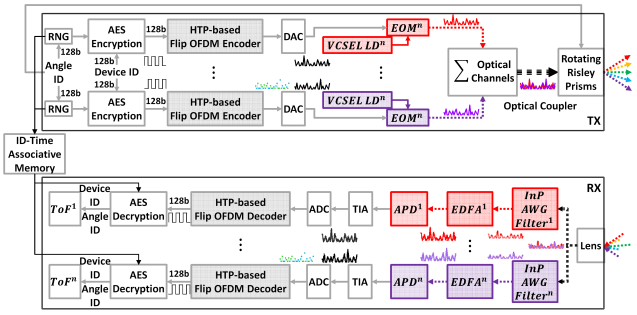

FIGURE 11. Block diagram of the proposed LiDAR with Risley prism and OOFDMA.

accuracy and reliability of the measurements [62]. Most OOFDMA approaches employ the inverse discrete Fourier transform (IDFT) and DFT for multiplexing/demultiplexing of the subchannels. As shown in Figures 9 and 10, this study uses DHT or inverse DHT (IDHT) to multiplex and demultiplex the subchannels, provided that the input alphabets are drawn from real constellations such as Mary pulse amplitude modulation (PAM). The kernel for both DHT and IDHT is identical, so the same algorithm can perform both processes. Unlike conventional approaches that require Hermitian symmetric (HS) in the frequency domain (FD) to obtain a real-valued time domain (TD) signal, the proposed method generates a real-valued output for DHT/IDHT when a real-valued input is provided. By controlling the power of the emitted laser, it is possible to measure at different distances. Distance is measured by the signal's flight time, whereas the object's relative speed can be determined by measuring the Doppler shift of the subchannel. OOFDMA suffers from a high peak-to-average power ratio (PAPR) due to the constructive addition of subchannels, which can be a significant limitation for intensity modulation-direction detection (IM-DD) methods with class-1 lasers that have a maximum optical output power less than the accessible emission limit (AEL). The maximum permissible exposure (MPE) of class 1 designation for LiDAR indicates that the sensor's laser emissions are safe for human eyes. This classification ensures that the LiDAR can be used without posing a risk of eye injury, even under direct exposure. To address this issue, precoding techniques have been proposed for moderate PAPR reduction gain with small computational complexity, of which the discrete HTP-based flip-OFDM has superior PAPR performance [62]. Figure 9 shows the process of creating a transmission signal using OOFDMA as shown below, and Figure 10 shows the process of receiving a reflected wave in reverse order.

The proposed LiDAR uses advanced encryption standards (AES) and randomly generated device and angle identifiers to mitigate the risks associated with external threats. Since LiDAR's input and output signals are based on reflected waves, they are consistently exposed to external threats, making them susceptible to external threats and mutual interference [86]. To address this issue, the AES encryption method, which employs symmetric encryption, ensures the security of transmitted data without revealing the information. Using AES tokens as session keys provides a robust mechanism for establishing secure sessions between transmitting and receiving LiDAR pulse sequences. When a LiDAR initiates a session with a system, a session token is generated. This token is the session key and is encrypted using the AES algorithm with a secret key known only to itself. Upon receiving the encrypted session tokens, the LiDAR decrypts them using the appropriate AES decryption key. This process ensures that only authorized received pulse streams with the correct decryption key can establish sessions with the LiDAR. Session keys generated from AES tokens can be periodically renewed to increase security. It helps to reduce the risk of session hijacking or unauthorized access by ensuring that session keys have a limited lifetime. At the end of the session, the session key is securely discarded or invalidated to prevent further access. However, the decryption of received data using AES encryption requires prior knowledge of the AES token key. Therefore, when LiDAR transmits AES-encrypted data, only it can interpret them, resulting in high safety against external threats. The generated OOFDMA signals, as shown in Fig. 11, are connected to 128 vertical-cavity surface-emitting (VCSEL) laser diodes (LD) with DWDMA. DWDMA is a technique used in optical communication systems to enable multiple transmitters to share the air by assigning each transmitter a unique wavelength. The wavelengths selected for DWDMA should have sufficient spacing between them to minimize interference and crosstalk between channels. The spacing depends on factors such as the modulation format, signal bandwidth, and the characteristics of the optical components used in the LiDAR. It enables the simultaneous transmission of multiple laser pulse streams over the air. External optical modulators (EOMs) with different wavelengths produce transmit signals with different wavelengths. An optical coupler combines 128 optical streams into a single optical stream which is then inputted into the rotating Risley prism. The outputs of the optical coupler are incident on the Risley prism along its central axis through an optical cable. The Risley prism refracts each plurality of laser signals output by the optical coupler at a different angle according to the wavelength [47], [85]. It allows a plurality of laser signals with different wavelengths for the same device and angle identifier data to be simultaneously transmitted toward different target points. The transmitter changes the direction of the central axis in the 3D space by changing three rotating angles of the Risley prism.

A lens collects and gathers the incoming reflected laser pulse streams, ensuring the maximum laser is directed toward the receiver side. An Indium phosphide (InP) arrayed waveguide grating (AWG) is an optical device based on AWG technology constructed using InP as the substrate. This plays a crucial role in separating different wavelengths of reflected laser pulse streams for reception. After passing through the InP AWG, the weakened reflected laser pulse

streams are amplified using an Erbium-doped fiber amplifier (EDFA). An EDFA amplifies reflected laser pulse streams. The primary function of an EDFA is to boost the strength of optical signals that have weakened during transmission through air. The amplified signal is then converted to an electrical signal using Avalanche photodiodes (APDs) and transimpedance amplifiers (TIAs). APDs are photodetectors that operate based on the avalanche multiplication effect in a semiconductor material, and they produce a photocurrent in response to incident laser pulse streams. TIAs are an essential interface between the APDs and subsequent electronic processing stages. By converting the photocurrent to a voltage signal and amplifying it, the TIAs enable accurate and efficient processing of the reflected laser pulse streams, contributing to the overall performance of the LiDAR. After the analog-to-digital converter (ADC)s, the signals are passed through an HTP-based flip-OFDM decoder to convert them to the appropriate binary signals. Only signals that can be decrypted with the existing key are received during AES decryption and those that cannot are discarded to eliminate disturbances or interference from external signals. Angle identifier (ID) determines when the laser pulse stream was transmitted, derives the flight time, and calculates the distance.

B. PERFORMANCE EVALUATION

1) PROTOTYPE DESIGN AND EXPERIMENTAL SETUP

The performance was assessed by measuring distance and intensity with a 2 m × 2 m paper wall placed at a distance of 2.5 m in front of the prototype. Since LiDAR characteristics are strongly affected by bad weather [87], [88], such as rain and fog, we assumed clear weather for our experiments. Figure 12 shows the configured environment for the experiments. The distance measurement of the proposed LiDAR was carried out using the operation of the LiDAR described in Section IV-A

The prototype utilizes a coded laser pulse stream to identify the location and determine the distance to an object. The transmitter, running in MATLAB, generates an eight-bit stream comprising a five-bit identification number and a three-bit cyclic redundancy check (CRC) checksum from the most significant bit (MSB) to the least significant bit (LSB). The identification numbers represent the location in each bearing direction. The CRC-3 checksum is an error detection code to detect accidental changes and validate the received bit stream. The power of the laser pulse emitted in the steering direction is equal to or similar to the MPE of class 1 laser products. The four laser pulse streams are coded using the OOFDMA technique to generate a bit stream orthogonal to the other. The OOFDMA encoder saves coded laser pulse stream information when the leading laser pulse is emitted to calculate the ToF.

The generated OOFDMA signals are fed to three laser diodes with different wavelengths in TripleX-WSLS by analog modulation to produce transmission signals with different

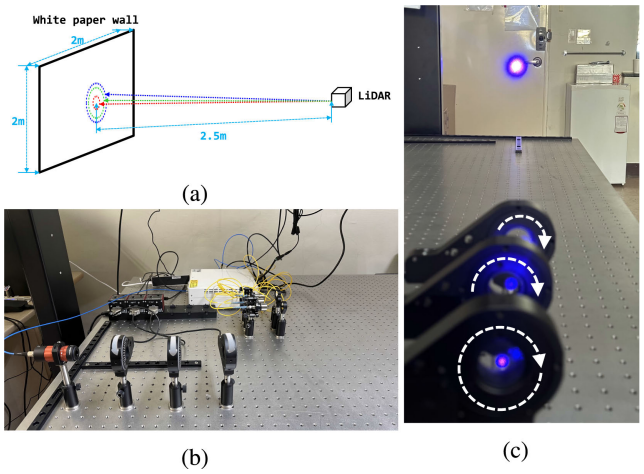

FIGURE 12. Experimental implementation of the prototype LiDAR. (a) Experimental environment; (b) The entire prototype LiDAR included a triple laser source, three high-speed photodetector modules, three round wedge prism, and a four-channel high-speed digitizer; (c) Three laser pulse streams are refracted in different directions through the Risley prism according to their wavelengths.

wavelengths. The TripleX-WSLS from the Wavespectrum Laser Group was chosen because it provides a triple-RGB fiber-coupled white laser source. The red (638 nm), green (520 nm), and blue (450 nm) lasers were integrated into a single fiber to provide the optimal white laser. It consisted of the LD, the LD driver, and a thermoelectric (TE) cooling part. Each wavelength was independently controlled by analog modulation. Three optical laser pulse streams are fed into optical couplers to combine three pulse streams into a single pulse stream. The combined laser pulse stream is transmitted in a Risley prism. The Risley prism consists of three 1-inch round wedge prisms from Thorlab (PS810-A, PS811-A, and PS-812-A), each using USB to control rotation. When a combined laser stream passes through the Risley prism, it undergoes refraction, which is the bending of laser streams as it passes from one medium to another. In this case, the laser streams pass through the optical material of the prisms. The wedge shape of the prisms causes the laser streams to change direction as they travel through the prisms. Finally, refracted laser pulse streams are steered in three directions according to their wavelengths.

Three receivers are equipped with a lens that receives the reflected pulse streams, which are then converted into a photocurrent using a high-speed photodetector. The resulting photocurrent of the photodetector is pre-amplified and converted into a voltage signal by a trans-impedance amplifier (TIA). We used three high-speed photodetectors, the PD1000-VIS from QUBIG, which can operate at a frequency up to 1 GHz with a gain of 16 kV A^{-1}. The photodetectors are a high-speed Si PIN photodiode designed to detect visible to near-infrared light with an optimum spectral range of 320 to 1000 nm. The amplified photodetectors have an integrated low-noise TIA that provides a fixed gain, resulting in a high signal-to-noise ratio (SNR).

The voltage signals are routed directly to a four-channel high-speed ADC. We chose an Express CompuScope PCIe Gen3 digitizer CSE161G4 from GaGe RazorMax. This digitizer has four 16-bit channels in 1 GS s^{-1} and 600 MHz bandwidth, with PCIe data streaming rates up to 5.2 GB s^{-1}. After the conversion, the receiving signal processor saves the arrival time and the digitized result to the memory queue. The receiver detects the matched OOFDMA pulse stream using an autocorrelation function of the memory queue. The digitized result is converted into an eight-bit stream in the decoded process. The receiver generates the CRC using a three-bit CRC algorithm that uses a five-bit identification number and compares this CRC with that included in the eight-bit stream. Suppose the two CRCs match. In that case, the receiver uses the identification number to identify the pulse emission time. Then, it calculates the time-of-flight and the distance between the LiDAR and the object. A point-cloud image is formed when these processes are performed for the entire set.

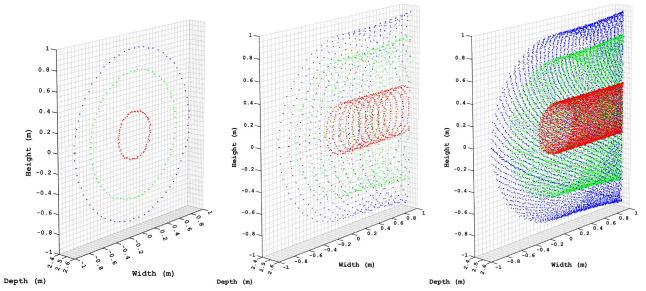

(a) Single rotation (b) Multiple rotation with coarse shift of center axis (c) Multiple rotation with fine shift of center axis

FIGURE 13. Measurement mechanism and the results obtained by operating the prototype using three laser pulse streams and a Risley prism. (a) A point cloud in which a Risley prism rotates one 360° and measures a paper wall. (b) After the Risley prism rotates once, the point cloud is measured by rotating the central axis of the Risley prism 1.8° to the right. (c) After the Risley prism rotates one time, the point cloud is measured by rotating the central axis of the Risley prism 0.18° to the right.

2) DISTANCE MEASUREMENT OF PAPER WALL

To verify the operation of the proposed LiDAR, the LiDAR was operated in the manner proposed in the environment shown in Figure 12. Three laser pulse streams enter the central axis of the Risley prism. They are refracted at different angles depending on the laser's wavelength, the prism's refractive index, the prism, the angle of the prism, and the spacing of the prisms. With the central axis of the Risley prism fixed, the object is measured once, and then the three prisms are simultaneously rotated by 0.5° to select the next measurement object. After measuring a total of 72 times, a 360° rotation is completed, and scanning is performed in a pattern as shown in Figure 13(a). The wavelength of the laser determines the spacing between the three laser pulse streams, the refractive index of the prism, the angle of the prism, and the spacing of the prisms. Changing these factors can vary the scanning pattern. After making one rotation with the prism's central axis fixed, the prism's central axis is rotated 1.8° to the right and then measured while rotating 360° around the central axis. If the same operation is repeated, scanning is performed in the same pattern as Figure 13(b). After making one rotation, the central axis of the prism is rotated to the right by 0.18° and then measured while rotating 360° around the central axis. The results measured with this scanning pattern appear in Figure 13(c). The smaller the angle at which the central axis is rotated to the right, the more precise measurements can be made. Still, the measurement time increases proportionally as the measurement interval decreases. Traditional scanning LiDAR measures one line vertically, but the proposed LiDAR measures one line in a circle by rotating the Risley prism. If we move the central axis to the right, we can measure multiple lines continuously instead of just one line. Depending on the distance, if we move more than a certain angle to the right, we can measure the target near the previously measured position and measure the target more precisely.

C. PERFORMANCE COMPARISON

To compare the performance of LiDARs, the prototype was tested in five different modes [64]. Although all LiDARs have the same laser wavelength and pulse width, they differ in the encoding method and the pulse stream. The length, pulse count, and pulse position in the pulse stream depend on the pulse coding method employed by the LiDAR instrument. As a result, it determines the time and power required to emit and receive the pulse stream to measure a point. The image resolution and frame refresh rate depend on the transmission time, while the maximum measurement distance depends on the pulse power. We present the behavioral characteristics of five different LiDAR sensors to evaluate performance against the proposed LiDAR, and detailed operational parameters are given in Table 2.

We tested the proposed LiDAR prototype in five modes to evaluate the accuracy and precision of the distance under different operating conditions, as presented in Table 2. Using white paper placed 2.5 m from the LiDAR, 1000 measurements were obtained, as carried out in [64]. The accuracy and precision of the position were measured for the five LiDARs according to the standards of the American Society for Photogrammetry and Remote Sensing (ASPRS) [89]. The distance measurement results vary for different LiDARs, and the line becomes longer as the error increases. Pulsed LiDAR, which uses only one pulse, has the highest error and the lowest number of pulses, as shown in Figure 14(a) and Figure 15(b). Sequential firing LiDAR in Figure 14(b) and Figure 15(b), on the other hand, uses the largest number of pulses and has the smallest error. The unipolar concurrent firing LiDAR in Figure 14(c) and Figure 15(c) and the bipolar concurrent firing LiDAR in Figure 14(d), and Figure 15(d) use fewer pulses than the sequential firing LiDAR, but their range errors are similar. The range error decreases as the number of measurement pulses increases, but the

TABLE 2. Characteristics of five LiDARs.

Item		Pulsed LiDAR	Sequential firing LiDAR	Unipolar concurrent firing LiDAR	Bipolar concurrent firing LiDAR	OOFDMA concurrent firing LiDAR (Proposed)
Beam steering mechanism		Body rotation	MEMS mirror tilting	Body rotation	Body rotation	Body rotation with Risley prism
Rotation per second		10	10	10	10	10
Lateral angular resolution		0.191 88°	0.3149°	0.0036°	0.002 16°	0.0018°
Firing cycle time		2.665 µs	6.1 µs	1 µs	0.6 µs	0.5 µs
Dwell time		53.3 µs	781.25 µs	1 µs	0.6 µs	0.5 µs
Field-of-View	Azimuth	360°	40°	360°	360°	360°
	Elevation	40°	40°	40°	40°	40°
Laser beam	Firing mechanism	One pulse	1D-OCDMA coded pulses	2D-OCDMA coded pulses	2D-OCDMA coded pulses	OOFDMA coded pulses
	Wavelength	903 nm	903 nm	903 nm	903 nm to 1568.3623 nm	903 nm to 1568.3623 nm
	Channel	128	128	128	128	128
Spreading method	Coding scheme	N/A	Asynchronous prime sequence code	Carrier-hopping prime code	Code-inversion keying prime permuted code	Discrete Hartley transform based flip-OFDM
	Factor	N/A	Weight 11, length 121	Weight 3, length 11	Weight 3, length 4	4-PAM, 2 subcarrier
	Number of wavelength	1	1	3	4	1
	Line code	N/A	Unipolar NRZ	Unipolar NRZ	Bipolar NRZ	PAM
Pulse stream	Length	N/A	9-bit	9-bit	8-bit	8-bit
	Format	N/A	1-bit SoF, 5-bit ID, 3-bit CRC	1-bit SoF, 5-bit ID, 3-bit CRC	5-bit ID, 3-bit CRC	5-bit ID, 3-bit CRC
	Transmitting method	8 channel at once, 16 transmitting groups	One chip by one chip in sequentially	All channels in concurrent, All wavelengths in concurrent, One chip by one chip in sequentially	All channels in concurrent, All wavelengths in concurrent, One chip by one chip in sequentially	All channels in concurrent, All wavelengths in concurrent, One chip by one chip in sequentially
	Number of time bin	1	1089	99	24	4
	Number of pulse	1	99	27	48	4
	Transmitting time	5 ns	5445 ns	495 ns	120 ns	20 ns
References		[27]	[35], [78], [79]	[38], [71]	[41]	[64]

error levels remain constant once the number exceeds a certain threshold. The range error decreases as the number of measurement pulses increases. The increased number of pulses also leads to a longer pulse transmission time, resulting in longer measurement and computation times. The method proposed in this study, given in Figure 14(e) and Figure 15(e) uses OOFDMA, and four pulses for one location, results in the second shortest pulse transmission time among the five LiDARs. However, the method measures distance with more than twice the accuracy of the single-pulse method. The experimental results for point cloud density, precision, and distance precision are summarized in Table 3 for a better presentation. Among the five LiDARs, the OOFDMA concurrent firing LiDAR proposed in this paper exhibits the best characteristics. It has the shortest measurement time and the highest point cloud density, which enables the most precise three-dimensional measurement of the desired area. While the proposed LiDAR exhibits these good characteristics, the number of pulses transmitted is the lowest among the concurrent firing LiDARs, resulting in an excellent maximum measurement distance.

V. VARIABLE FIELD-OF-VIEW SCANNING ON REGION OF INTEREST

In the proposed LiDAR shown in Figure 11, 128 laser diodes and EOMs with varying wavelengths are utilized to produce transmit signals with different wavelengths. These signals are combined as an optical stream using an optical coupler and input to the rotating Risley prism along its central axis through an optical cable. The Risley prism refracts each

TABLE 3. Comparison of experimental result.

Item		Pulsed LiDAR	Sequential firing LiDAR	Unipolar concurrent firing LiDAR	Bipolar concurrent firing LiDAR	OOFDMA concurrent firing LiDAR (Proposed)
Measurement time (ms)		28.782	100	7.112	8.5338	6.12
Pulse count		69 120	354 816	24 579 072	87 386 112	6 266 880
Point cloud density		1003	507	8513	17 173	17 768
Distance accuracy (m)		0.047 266	0.029 269	0.029 583	0.029 175	0.029 170
Distance precision (m)		0.019 134	0.002 870 1	0.003 686 7	0.002 764 1	0.002 759 8
Distance error (m)		0.054 934	0.027 013	0.031 656	0.029 553	0.027 578
Maximum distance (m)	Black wall	78	92	131	92	242
	White wall	237	277	394	278	534
Related figures		14(a), 15(a)	14(b), 15(b)	14(c), 15(c)	14(d), 15(d)	14(e), 15(e)

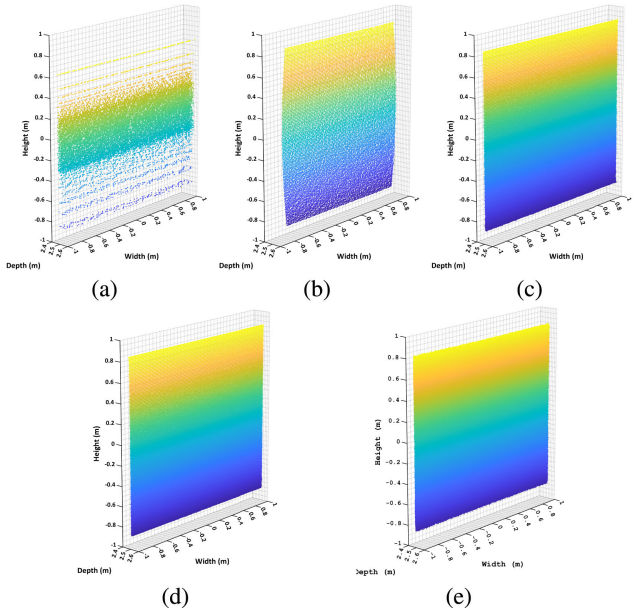

FIGURE 14. 3D point cloud generated by the five LiDARs. (a) Legacy pulsed LiDAR 128 channels based on body rotation. (b) Sequential transmission LiDAR based on MEMS mirror tilt and 1D unipolar optical codes. (c) Concurrent transmitting LiDAR based on body rotation and 2D unipolar optical codes. (d) Concurrent transmitting LiDAR based on body rotation and 2D bipolar optical codes. (e) Concurrent transmitting LiDAR based on the Risley prism and OOFDMA.

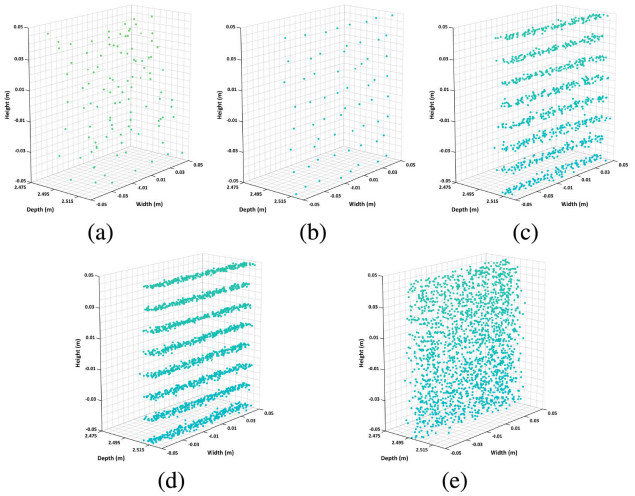

FIGURE 15. Central point zoomed 3D point cloud generated by the five LiDARs in Fig. 14. (a) Legacy 128 channel pulsed LiDAR based on body rotation. (b) Sequential transmitting LiDAR based on MEMS mirror tilting and 1D unipolar optical codes. (c) Concurrent transmitting LiDAR based on body rotation and 2D unipolar optical codes. (d) Concurrent transmitting LiDAR based on body rotation and 2D bipolar optical codes. (e) Concurrent transmitting LiDAR based on Risley prism and OOFDMA.

laser signal at a different angle based on its wavelength, allowing every pulse stream with different wavelengths to be transmitted in different target directions while maintaining encrypted identifiers, as presented in Figure 8. The direction of the central axis can be changed in a 3D space by altering the three rotating angles of the Risley prism. The measurements are taken around the Risley prism's center axis by its rotation angle. As the center axis moves to the side, the target directions overlap, allowing very dense measurements, as depicted in Figure 13.

Here, we discuss how the rotation of LiDARs can be optimized to detect obstacles in the UAM context. Analysis reveals that each LiDAR rotates 360° based on the central axis of the prism for the measurement direction. It detects surrounding obstacles while rotating 360° based on the center of the UAM equipped with LiDAR (Figure 16(a)). Furthermore, we demonstrate that obstacle detection can be improved by deploying multiple LiDARs, which can divide the 360° FoV into equal parts, thus increasing the detection speed (Figure 16(b)). Furthermore, we propose the use of overlapping LiDARs to detect small obstacles in a specific direction (Figure 18(a)). This technique can be beneficial for detecting obstacles in the air, which are often small and difficult to detect with a single LiDAR.

To understand the surrounding environment, the existing LiDAR rotates around the z-axis in a spherical sinusoidal system 360° and transmits and receives laser pulses in each direction. The proposed LiDAR uses a Risley prism and has two independent rotation axes. One rotation axis is the center

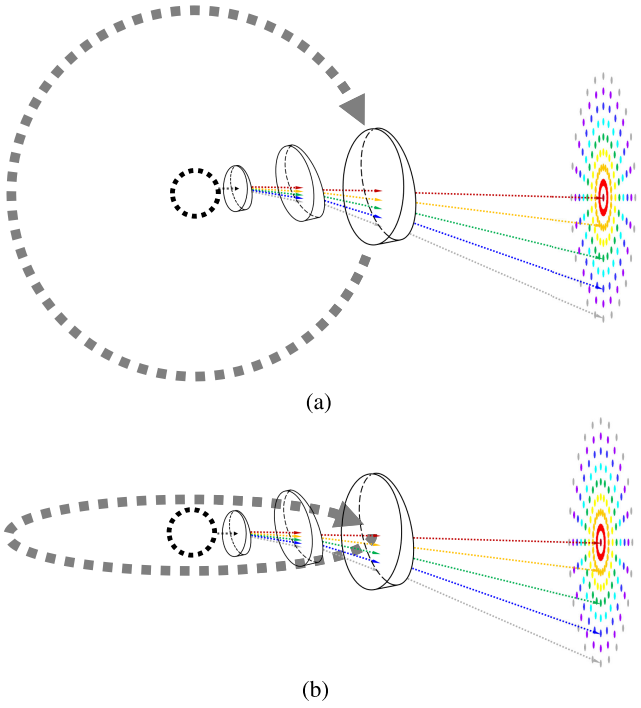

FIGURE 16. The proposed LiDAR uses two axes that rotate 360° to scan the front and surrounding environment. The scanning operation is seen from above (a) and from the side (b).

of the Risley prism and the central axis is around the prisms that make up the Risley prism, which rotate individually. The Risley prism rotates 360° in each direction to transmit and receive laser signals to detect objects. Another axis is the z-axis of the spherical coordinate system, like existing LiDARs, and is the axis around which rotates the entire transmitting and receiving unit of the LiDAR, which is composed of a Risley prism, 360°. As shown in Figure 16, the entire 360° environment around the LiDAR can be scanned along with the front 360°.

The proposed LiDAR uses an OOFDMA-based optical signal processing technique to encode the measurement direction information into a different code for each transmitted signal. Laser signals encoded with OOFDMA can be decoded without knowing the code. Suppose different LiDARs use various codes and do not share them. In that case, the receiver ignores the laser signals transmitted from different LiDARs because they cannot be decoded even if they hit an object and are received. In other words, only the laser signal transmitted by the device can be decoded, so even if multiple LiDARs operate simultaneously, only their signals can be distinguished, so mutual interference does not occur. Applying this approach can provide various operational advantages by using multiple LiDARs simultaneously instead of one LiDAR when scanning the surrounding environment.

As shown in Figure 17(a), the existing LiDAR sensor detects surrounding obstacles while rotating 360°. The ability to detect surrounding obstacles is greatly affected by the performance of LiDAR, which operates alone. The

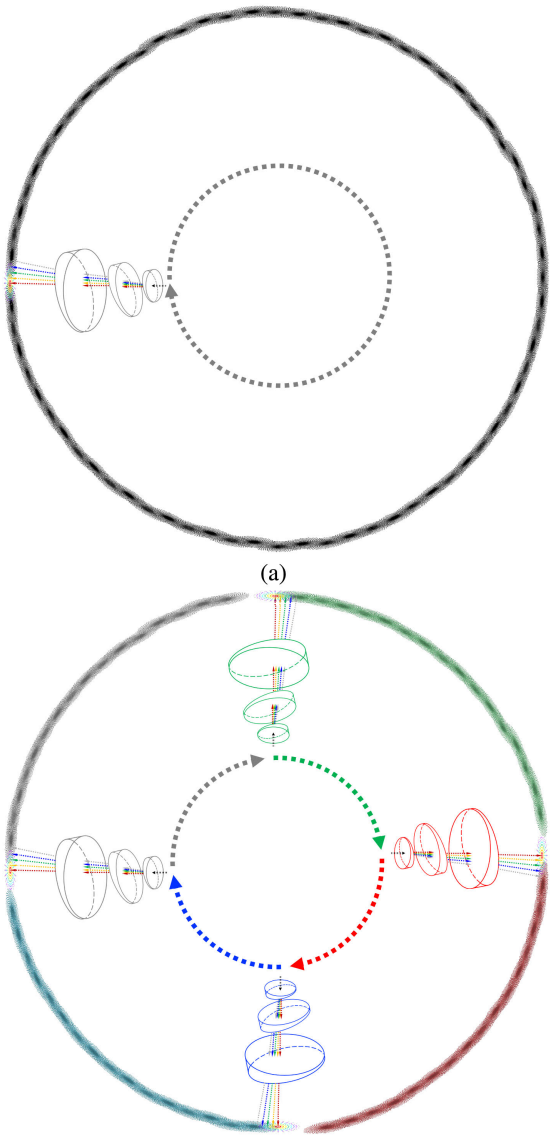

FIGURE 17. Different methods for rotating LiDAR to detect surrounding obstacles. In (a), the LiDAR rotates 360° based on the center of the urban air mobility (UAM) vehicle equipped with the LiDAR, with rotation based on the central axis of the prism. In (b), multiple LiDAR operate simultaneously by dividing 360° into equal parts based on the number of LiDAR.

ability to detect surrounding obstacles is determined by the characteristics of the lidar, such as its maximum measurement distance, FoV, resolution, refresh rate, and rotation speed. When multiple LiDARs can be operated simultaneously, multiple sensors can divide the area to be scanned. Therefore, the performance of several LiDARs rather than one LiDAR collectively determines the overall obstacle detection ability. Figure 17(b) shows a case where four LiDARs operate simultaneously. When multiple LiDARs detect obstacles by dividing the area like this, all areas can be detected even if the rotation speed is lowered to 25% so that maximum measurement can be achieved. Other performance

metrics, such as distance, FoV, resolution, refresh rate, etc., can be increased. Using more LiDARs simultaneously can further increase the maximum measurement distance, FoV, resolution, and refresh rate while lowering the individual rotation speeds of the LiDARs, further expanding the ability to detect obstacles in the surroundings.

In LiDAR's main application areas, such as self-driving cars, autonomous walking robots, and UAM, detecting obstacles in the direction of travel is more important than detecting obstacles in the surrounding environment. Suppose there is an obstacle in the direction of travel. In that case, recalculating the movement path is necessary, so it is beneficial to precisely identify the obstacle ahead as quickly as possible. Sometimes, obstacles are concentrated in a specific direction, so it is necessary to use LiDAR to scan a particular direction with very high performance. LiDAR using a Risley prism can rotate the internal prism and adjust the distance between prisms. The longer the distance between prisms, the greater the refraction of the laser signal, creating a larger scanning area. When multiple LiDARs are used at the same time to detect obstacles, more specifically, at a specific location in a particular direction, the distance between the prisms or the angle of the internal prism is adjusted according to the distance between the obstacle and the LiDAR to detect the obstacles with better characteristics. Multiple LiDARs focus on a specific direction where an obstacle is located, but the focusing method can differ depending on the obstacle's size or distribution characteristics.

In this study, four different LiDAR sensor scanning schemes are presented and compared to measure 500 m ahead, as shown in Figure 19 and Table 4. Figure 19(a) shows a single LiDAR sensor, while Figure 19(b) through Figure 19(d) depict four LiDAR sensors working together. In Figure 19(a), 19(b), and 19(c), the scanning scheme becomes the same hollow circles, where the three prisms have the same angular velocity ($\omega_1 = \omega_2 = \omega_3$), rotation angle ($\theta_1 = \theta_2 = \theta_3$), and prism spacing ($D_1 = D_2$). However, when the angle difference ($\theta_{\Delta 1}$ *and* $\theta_{\Delta 2}$) and the prism distance of the prisms of the four LiDAR sensors are different, the angle difference between the prisms is closer to 180° in the inner hollow circle and the angle difference between the prisms is closer to 0° in the outer hollow circle. The larger the hollow circle, the farther the prism distance; the smaller the hollow circle, the closer the prism distance.

The proposed LiDAR, as shown in Figure 11, comprises three fused silica wedge prisms with the same refractive index, which depends on the wavelength of the emitted laser pulses ($1.426323 \leq n_\lambda \leq 1.460689$), the same wedge angle ($\alpha_1 = \alpha_2 = \alpha_3 = 10°$), and the same thinnest end thickness ($T_1 = T_2 = T_3 = 10\,\text{mm}$) but has different diameters ($d_1 = 50\,\text{mm}, d_2 = 75\,\text{mm}, d_3 = 100\,\text{mm}$). This study focuses on evaluating the feasibility of the proposed LiDAR for obstacle detection and the effectiveness of the Risley prism in improving the accuracy and precision of distance measurement. The simulation results demonstrate that the proposed LiDAR can effectively detect obstacles and has

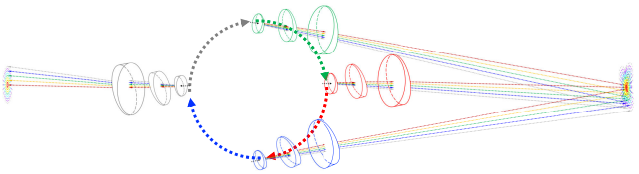

(a) Scanning focused on a specific area in front

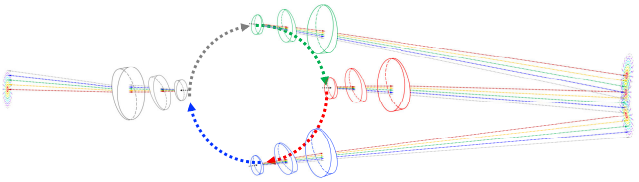

(b) Scanning slightly wider in a specific area in front

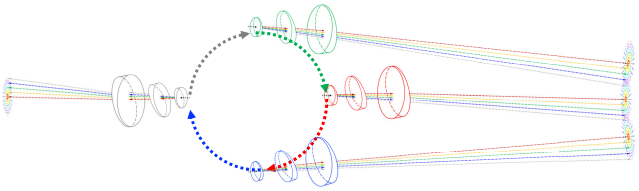

(c) Scanning scattered across a wide area ahead

FIGURE 18. The method of operating LiDAR together can differ depending on the size and distribution of the object to be detected ahead. (a) Suppose that a tiny object is in a specific area in front. In that case, many characteristics of the object can be detected if as many LiDARs as possible are focused on scanning that area. (b) If the object is slightly larger or spread over a slightly larger area, the object can be detected by scanning several LiDARs in a partially overlapping form. (c) If the object is spread over a large area, the object can be detected well by scanning multiple LiDARs in succession.

significant potential for practical applications. Simulations are carried out using Synopsys RSoft OptSim optical simulation software and MathWorks MATLAB R2023b [64], [71], [78], [90]. We added optical characteristics related to the Risley prism [47], laser transmission and reception, as well as encoding and decoding, signal processing, intensity calculation, and distance calculation tasks [61], [63], [78]. Simulations involve various scanning schemes for the LiDAR, including a single LiDAR sensor and four LiDAR sensors working together.

The default behavior of the LiDAR is shown in Figure 19(a), which scans only the part corresponding to the wall of a circular space with a diameter of approximately 180 m. However, this scanning scheme has a large minimum channel spacing and an angular spacing of adjacent channels, making it difficult to detect small objects and leaving a sizable and unmeasurable area because of the blank space in the middle. This study proposes various scanning patterns and densities to overcome these limitations. If an obstacle is detected while scanning obstacles in the front using one LiDAR, the scanning pattern and density can be changed in various ways, and multiple LiDAR sensors can be operated simultaneously to enable specific recognition of the obstacle. If four LiDAR sensors are used as overlap, it is possible

TABLE 4. Characteristics of representative commercial LiDARs.

Item	Basic scanning scheme	Interleaved scanning scheme	Diagonal scanning scheme	Continuity scanning scheme
Related Figure	Fig. 19(a)	Fig. 19(b)	Fig. 19(c)	Fig. 19(d)
Number of LiDAR	1	4	4	4
Height	181.050 m	181.050 m	256.982 m	253.814 m
Width	180.094 m	180.094 m	256.909 m	253.814 m
Angle interval	4°	1°	4°	4°
Target points	46 080	184 320	184 320	184 320
Minimum channel spacing	0.167 m	0.167 m	0.167 m	0.084 m
Minimum angular spacing	4.763 m	1.628 m	4.763 m	3.114 m
Wall thickness	24.2799 m	24.2799 m	24.2799 m	101.689 m
ROI scanning coverage	16.3 %	16.3 %	39.1 %	66.6 %

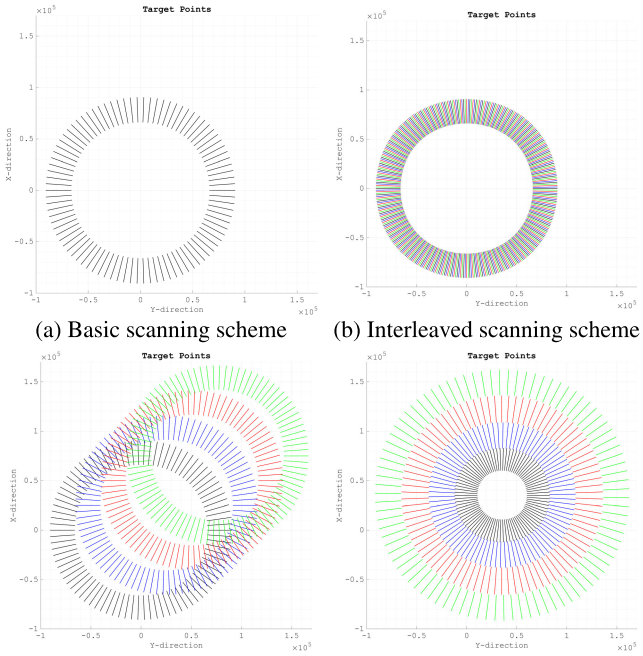

(a) Basic scanning scheme (b) Interleaved scanning scheme

(c) Diagonal scanning scheme (d) Continuity scanning scheme

FIGURE 19. Variable FoV scanning schemes according to obstacles. Four LiDARs cooperate to change the measurement radius and pattern according to the size and distribution of obstacles and the region of interest (ROI). (a) shows the basic scanning scheme in which one LiDAR operates independently. (b), (c), and (d) show interleaved, diagonal, and continuity scanning schemes, respectively, in which four LiDARs work together to scan ROI.

to scan the same space four times densely, as shown in Figure 19(b). In Figure 19(c), the prism center axis of the four LiDAR sensors is aligned, but the measurement angles are slightly offset at regular intervals. Compared to Figure 19(a), the measurement angle interval is reduced by a quarter, allowing smaller objects to be detected. If four LiDAR sensors are used together, the space that one LiDAR cannot measure can be measured by another LiDAR, and most of the area can be scanned, as shown in Figure 19(c). To reduce the space generated by the hollow circle, a scanning pattern is proposed in which four LiDAR sensors with the same axis reduce the size of the scanning circle, as shown in Figure 19(d). Figure 19(c) shows the prismatic center axes of the four LiDAR sensors arranged diagonally at regular intervals. The measurement channel and angle spacing are the same as shown in Figure 19(a). However, adjacent LiDAR sensors overlap, which can significantly reduce the blank space in the middle. In Figure 19(d), the prismatic center axes of the four LiDAR sensors are aligned, but the measurement radii are different. Other LiDAR sensors can compensate for the unmeasurable area in the middle of the LiDAR sensor measurement area, enabling obstacle detection over a large area.

VI. APPLICATION AREA AND FURTHER RESEARCH

LiDAR is most often used in autonomous vehicles to determine the available driving space. Cameras only produce 2D images and cannot determine distance, and radar has low resolution, making it difficult to accurately determine the space that can be moved. LiDAR generates 3D images at high resolution, which makes it most suitable for identifying operational space. To use LiDAR in self-driving cars, the mounting location is very important. The more parts it can be mounted on, the better, but it is very burdensome due to the size and price of the lidar. Since the cloud path of an autonomous car varies depending on the object in front, it is very advantageous to install LiDAR at least in front, and the best place is to integrate it with existing headlights. The headlights are always facing forward and the space is very large, making it advantageous to mount a lidar. When fusion of existing LiDAR, laser signals are transmitted to a desired location using a mirror, and laser signals reflected from an object are also received using a mirror. Mirrors are large in size and vulnerable to shock and vibration, so using them in headlights requires separate space and a method to prevent damage. The mirror's operating angle is small, limiting the scanning area. The Risley prism LiDAR proposed in this paper does not require a mirror but only space for the prism, so it requires much less space than the mirror method,

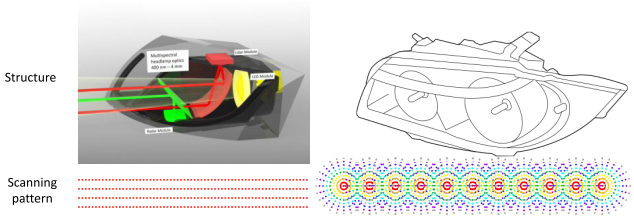

(a) When combining existing lidar with headlight (b) When the proposed lidar is combined with the headlight

FIGURE 20. Using existing LiDAR in headlights requires a mirror, which takes up a lot of space and is less reliable. There is little space for the mirror to move, so it is very difficult to scan the front efficiently. The proposed Risley prism-based lidar only requires space for the prism, and can actively respond to various objects by adjusting the inside of the Risley prism.

as shown in Figure 20. Additionally, by adjusting the internal prism rotation characteristics and spacing of Risley prisms, an active response is possible according to the characteristics of the object.

Obstacles in the area where aircraft or drones operate differ greatly from those of self-driving cars. In the case of self-driving cars, obstacles are attached to the ground and the moving speed is often slower than that of self-driving cars. In addition, the space where cars drive is often controlled by the law. In contrast, in airplanes and drones, very small and fast-moving obstacles, like birds, sometimes appear suddenly, and it is very difficult to predict in advance where they will appear in 3D space. In addition, in the case of high-voltage transmission lines built in mountains or large flat areas, they are difficult to detect because their thickness is thinner than that of other obstacles. Although these obstacles can be detected using a camera, it is more advantageous to use LiDAR because it is difficult to determine the distance. The existing LiDAR has a resolution lower than FoV, so detecting small objects in the air is difficult. Additionally, the refresh rate is very low, making it more difficult to detect fast moving objects. As presented in Figure 21, the proposed LiDAR has a larger FoV, high resolution, and high refresh rate compared to existing LiDAR, which makes it very advantageous for detecting aerial obstacles. Additionally, if multiple LiDARs are used simultaneously, higher resolution and refresh rates are possible, creating 3D images of similar quality to those of cameras. Even long and thin obstacles, such as high voltage transmission lines, can be detected without exception.

General aircraft operate at a height close to the city center only during take-off or landing. However, the UAM is a small airplane that operates in the city center and moves at a height similar to that of a helicopter. The city center is divided into commercial, industrial, and residential areas, each with its own characteristics. Commercial areas have many buildings and cars, and industrial areas generate a lot of heat due to factory facilities, but residential areas have fewer buildings and relatively lower temperatures. Commercial or industrial areas have higher temperatures than surrounding areas, leading to clear air turbulence (CAT) as shown in

FIGURE 21. If an aircraft encounters an unexpected bird, a dangerous situation may occur in which the engine, etc. are damaged. Small drones must operate at a height slightly above the ground and detect high-voltage transmission lines that are not at the altitude at which regular aircraft operate as obstacles.

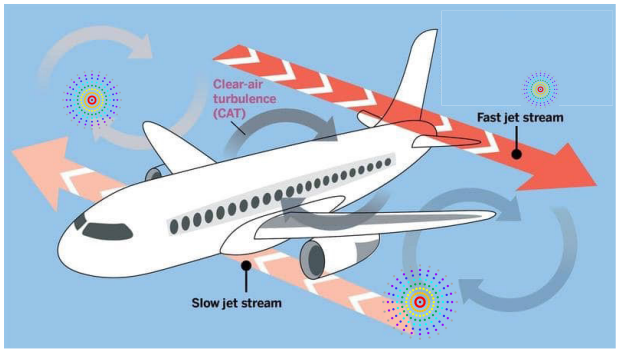

FIGURE 22. Clear air turbulence (CAT) emerges in a cloudless sky where fast and slow jet streams collide. It can neither be seen nor detected by radar. CAT can occur in urban areas and its impact on UAM.

Figure 22. Large aircraft are rarely affected by CATs that occur in urban areas due to their operating altitude and size. However, UAMs are greatly affected by CAT because they are small aircraft that operate at very low altitudes. CAT is invisible to the eye, so it is difficult to determine whether it occurs even with a camera. The proposed LiDAR can determine the moving speed of an object by identifying changes in continuous laser signals in the OOFDMA signal. When CAT occurs, dust in the city reacts and there is a rapid and irregular movement of dust. Suppose no obstacles are recognized by the camera and a Doppler effect occurs in a wide area when a signal transmitted through OOFDMA is received. In that case, it can be considered a CAT, and the route can be avoided in advance.

A golf ball with a diameter of about 4 cm moves at 300 km s^{-1} the moment it is hit by a driver, and a baseball ball with a diameter of about 7 cm moves at 200 km s^{-1} the moment it is hit by a batter's bat. Small objects move at very high speeds, making it difficult to track their trajectories with machines. In the case of sports broadcasts, the trajectories are generally tracked based on the experience of the person filming the video. In some cases, the ball's trajectory can be tracked well, but in other cases, it predicts in the wrong direction and cannot track the ball at all. The LiDAR proposed in this paper can operate multiple LiDARs simultaneously in various ways. In particular, depending on the situation, it is operated in the form of Figure 23, allowing the trajectory of even small, fast-moving objects to be tracked.

(a) Tracking the trajectory of a golf ball

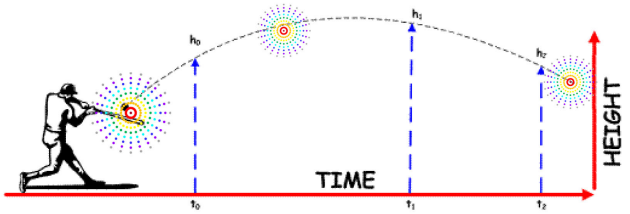

(b) Tracking the trajectory of a baseball ball

FIGURE 23. It is difficult to track fast-moving small objects like golf balls or baseballs. Since the proposed method can operate multiple LiDARs simultaneously, it is very advantageous to determine the actual movement of the ball by placing it in advance on the normal trajectory of (a) a golf ball or (b) a baseball ball.

VII. DISCUSSION

Scanning LiDAR technology presents numerous benefits but has several constraints that can affect its performance and applications. Scanning LiDAR sensors may encounter limitations in range capabilities, particularly for long-distance detection tasks. Ground-based scanning LiDARs adhere to MPE class 1 compliance to ensure human safety, resulting in restricted laser intensity emission and, consequently, a limited maximum measurement distance. Moreover, achieving high resolution demands denser point clouds, which may reduce the effective range of the LiDAR sensor. Conversely, extending the range might compromise spatial resolution.

Unlike radars and cameras, which predominantly utilize semiconductors, scanning LiDARs rely much on semiconductors but integrate mechanical and optical components. This complex synthesis increases production complexity and costs while imposing operational constraints. These components' precise calibration and alignment are crucial for reliable operation and accurate data capture, necessitating time-consuming processes and specialized equipment. Such intricacies increase manufacturing costs and introduce potential PoF, underscoring the importance of your expertise in this field.

Although cameras receive light wavelengths within the visible band, LiDAR also detects the near-infrared band adjacent to visible light. However, the short wavelength of visible light makes penetrating obstacles such as water difficult. Such limitations persist in environments where human vision is restricted, curtailing its efficacy. Adverse weather conditions, such as fog, rain, or dust, further diminish the effective range by scattering or absorbing laser beams, and obstacles obstruct the measurement behind them. Additionally, vibrations can compromise accuracy and reliability, particularly in outdoor or industrial settings.

LiDAR has low transmittance, limiting its functionality to structures directly connecting to the outside world for signal transmission and reception. While cameras do not transmit signals, LiDAR does, engaging in direct contact with the external environment by transmitting signals and receiving reflected signals. Scanning LiDARs boasting a 360-degree FoV rotating around a central axis requires extensive contact with the external environment. Contaminants such as dust, dirt, water droplets, or snowflakes adhering to these external surfaces can impede regular operation. LiDAR sensors must detect and eliminate contaminants from signal-transmitting and -receiving surfaces. Features such as brushes, air jets, or ultrasonic cleaners can remove contaminants without compromising sensitive components.

Despite the constraints, the potential for scanning LiDAR technology remains high. Understanding and addressing these limitations is crucial to optimizing performance and broadening its applicability across diverse industries and applications. Continuous research and technological advancements work tirelessly to alleviate these limitations and unlock novel LiDAR-based sensing and mapping capabilities.

VIII. CONCLUSION

The LiDAR technology has gained significant attention in recent years for aerial applications, especially with the advent of UAMs. However, traditional LiDAR with a fixed FoV is unsuitable for UAM operations because of the varying size and speed of the aerial objects. To address this limitation, developing the FoV LiDAR variable is crucial for UAM applications. Using a Risley prism in LiDAR technology provides a compact and versatile scanning sensor for various applications. The proposed LiDAR utilizes HTP-based flip-OFDM to generate a laser pulse stream and a Risley prism for steering. It incorporates a variable FoV function that adjusts the scanning pattern and density of the point cloud to correspond to different sizes, distances, and distributions of objects.

Using various techniques, such as AES and randomly generated identifiers, the proposed LiDAR ensures accurate and reliable measurements while minimizing mutual interference between laser signals. The development of variable FoV LiDAR can significantly improve the reliability and accuracy of LiDAR technology in aerial applications, enabling the development of more advanced UAM sensors for various applications. The proposed LiDAR's advanced encryption and identification techniques ensure the security of the transmitted data and prevent mutual interference between laser signals. LiDAR is vital for autonomous cars, and with Risley prism technology space needs for installing LiDAR can be achieved. The proposed LiDAR

excels at detecting fast-moving aerial obstacles in aircraft, offering high resolution and refresh rates. Multiple LiDARs enhance the image quality for thin structures, such as high-voltage lines. These advancements in LiDAR technology can potentially revolutionize how we gather information about the environment and improve the safety of UAM operations. The proposed LiDAR is a promising step towards more advanced and versatile LiDAR sensors that can be used in various applications, such as environmental monitoring, infrastructure inspection, and search and rescue operations.

The following abbreviations are used in this manuscript:

2D Two-Dimensional
3D Three-Dimensional
ADC Analog-to-Digital Converter
AEL Accessible Emission Limit
AES Advanced Encryption Standard
APD Avalanche PhtoDiodes
AWG Arrayed Waveguide Grating
CDMA Code-Division Multiple Access
CHPC Carrier-Hopping Prime Code
CRC Cyclic Redundancy Check
DFT Discrete Fourier Transform
DHT Discrete Hartley Transform
DWDMA Dense Wavelength Division Multiple Access
EDFA Erbium-Doped Fiber Amplifier
EOM External Optical Modulator
FD Frequency Domain
FoV Field-of-View
FoR Field-of-Regard
HS Hermitian Symmetric
HTP Hartley Transform Precoded
ID IDentification
IDFT Inverse Discrete Fourier Transform
IM-DD Intensity Modulation-Direction Detection
InP Indium Phosphide
LD Laser Diode
LiDAR LIght Detection And Ranging
LSB Least Significant Bit
MEMS Micro Electro Mechanical Systems
MPE Maximum Permissible Exposure
MSB Most Significant Bit
NRZ Non-Return to Zero
OCDMA Optical CDMA
OOFDMA Optical Orthogonal Frequency-Division Multiple Access
PAM Pulse Amplitude Modulation
PAPR Peak-to-Average Power Ratio
PD PhotoDiode
PIN Positive-Intrinsic-Negative
PoF Point-of-Failure
PRF Pulse Repetition Frequency
radar RAdio Detection And Ranging
RF Radio Frequency
ROI Region Of Interest
SNR Signal-to-Noise Ratio
SoF Start-of-Frame
TD Time Domain
TE ThermoElectric
TIA TransImpedance Amplifier
ToF Time-of-Flight
UAM Urban Air Mobility
UAS Unmanned Autonomous Ship
UAV Unmanned Aerial Vehicle
USB Universal Serial Bus
VCSEL Vertical-Cavity Surface-Emitting Laser diodes

ACKNOWLEDGMENT

(Gunzung Kim and Imran Ashraf are co-first authors.)

REFERENCES

[1] P. Daukantas, "LiDAR in space: From Apollo to the 21st century," *Opt. Photon. News*, vol. 20, no. 6, pp. 30–35, 2009.
[2] C. L. Glennie, W. E. Carter, R. L. Shrestha, and W. E. Dietrich, "Geodetic imaging with airborne LiDAR: The earth's surface revealed," *Rep. Prog. Phys.*, vol. 76, no. 8, Aug. 2013, Art. no. 086801.
[3] M. Nilsson, "Estimation of tree heights and stand volume using an airborne LiDAR system," *Remote Sens. Environ.*, vol. 56, no. 1, pp. 1–7, Apr. 1996.
[4] T. Brandtberg, "Classifying individual tree species under leaf-off and leaf-on conditions using airborne LiDAR," *ISPRS J. Photogramm. Remote Sens.*, vol. 61, no. 5, pp. 325–340, Jan. 2007.
[5] W. E. Baker, G. D. Emmitt, F. Robertson, R. M. Atlas, J. E. Molinari, D. A. Bowdle, J. Paegle, R. M. Hardesty, M. J. Post, R. T. Menzies, T. N. Krishnamurti, R. A. Brown, J. R. Anderson, A. C. Lorenc, and J. McElroy, "LiDAR-measured winds from space: A key component for weather and climate prediction," *Bull. Amer. Meteorological Soc.*, vol. 76, no. 6, pp. 869–888, Jun. 1995.
[6] L. Thobois, J. P. Cariou, and I. Gultepe, "Review of LiDAR-based applications for aviation weather," *Pure Appl. Geophys.*, vol. 176, no. 5, pp. 1959–1976, May 2019.
[7] A. S. Chase, D. Z. Chase, and A. F. Chase, "LiDAR for archaeological research and the study of historical landscapes," in *Sensing the Past* (Geotechnologies and the Environment), 2017, pp. 89–100.
[8] P. Rodríguez-Gonzálvez, B. J. Fernández-Palacios, Á. Muñoz-Nieto, P. Arias-Sanchez, and D. Gonzalez-Aguilera, "Mobile LiDAR system: New possibilities for the documentation and dissemination of large cultural heritage sites," *Remote Sens.*, vol. 9, no. 3, p. 189, Feb. 2017.
[9] M. Buehler, K. Iagnemma, and S. Singh, *The 2005 DARPA Grand Challenge: The Great Robot Race*, vol. 36. Berlin, Germany: Springer, 2007.
[10] J. Levinson, J. Askeland, J. Becker, J. Dolson, D. Held, S. Kammel, J. Z. Kolter, D. Langer, O. Pink, and V. Pratt, "Towards fully autonomous driving: Systems and algorithms," in *Proc. IEEE Intell. Vehicles Symp. (IV)*, Jun. 2011, pp. 163–168.
[11] C. Mertz, L. E. Navarro-Serment, R. MacLachlan, P. Rybski, A. Steinfeld, A. Suppé, C. Urmson, N. Vandapel, M. Hebert, C. Thorpe, D. Duggins, and J. Gowdy, "Moving object detection with laser scanners," *J. Field Robot.*, vol. 30, no. 1, pp. 17–43, Jan. 2013.
[12] Y. Li and J. Ibanez-Guzman, "LiDAR for autonomous driving: The principles, challenges, and trends for automotive LiDAR and perception systems," *IEEE Signal Process. Mag.*, vol. 37, no. 4, pp. 50–61, Jul. 2020.
[13] W. Wei, *ToF LiDAR for Autonomous Driving*. IOP, 2023.
[14] S. Siewert, K. Sampigethaya, J. Buchholz, and S. Rizor, "Fail-safe, fail-secure experiments for small UAS and UAM traffic in urban airspace," in *Proc. IEEE/AIAA 38th Digital Avionics Systems Conference (DASC)*, Sep. 2019, pp. 1–7.
[15] H. Tang, Y. Zhang, V. Mohmoodian, and H. Charkhgard, "Automated flight planning of high-density urban air mobility," *Transp. Res. C, Emerg. Technol.*, vol. 131, Oct. 2021, Art. no. 103324.
[16] E. Aldao, L. González-de Santos, and H. González-Jorge, "LiDAR based detect and avoid system for UAV navigation in UAM corridors," *Drones*, vol. 6, no. 8, p. 185, Jul. 2022.
[17] A. Mathur, K. Panesar, J. Kim, E. M. Atkins, and N. Sarter, "Paths to autonomous vehicle operations for urban air mobility," in *Proc. AIAA*, 2019, p. 3255.

[18] P. Wang, "Research on comparison of LiDAR and camera in autonomous driving," *J. Phys., Conf.*, vol. 2093, no. 1, Nov. 2021, Art. no. 012032.
[19] I. Bilik, "Comparative analysis of radar and LiDAR technologies for automotive applications," *IEEE Intell. Transp. Syst. Mag.*, vol. 15, no. 1, pp. 244–269, Jan. 2023.
[20] J. Domhof, J. F. P. Kooij, and D. M. Gavrila, "A joint extrinsic calibration tool for radar, camera and LiDAR," *IEEE Trans. Intell. Vehicles*, vol. 6, no. 3, pp. 571–582, Sep. 2021.
[21] R. Ravindran, M. J. Santora, and M. M. Jamali, "Camera, LiDAR, and radar sensor fusion based on Bayesian neural network (CLR-BNN)," *IEEE Sensors J.*, vol. 22, no. 7, pp. 6964–6974, Apr. 2022.
[22] M. A. Abu-Rgheff, *Introduction to CDMA Wireless Communications*. Cambridge, MA, USA: Academic Press, 2007.
[23] M. U. Khan, M. S. Sharawi, and R. Mittra, "Microstrip patch antenna miniaturisation techniques: A review," *IET Microw., Antennas Propag.*, vol. 9, no. 9, pp. 913–922, Jun. 2015.
[24] P. F. McManamon, *Field Guide to LiDAR* (Field Guide), vol. 36. Bellingham, WA, USA: International Society for Optics and Photonics, 2015.
[25] P. F. McManamon, W. F. Buell, G. Kamerman, O. Steinvall, and K. Asai, "Active electro-optical sensing: Phenomenology, technology, and applications," *Opt. Eng.*, vol. 31201, May 2017.
[26] *Operating Instructions for Laser Meas. Sensors LMS5xx Product Family*, SICK AG, Waldkirch, Germany, 2015.
[27] *VLS-128 User Manual*, Velodyne LiDAR, San Jose, CA, USA, 2018.
[28] Y. Qin, T. T. Vu, and Y. Ban, "Toward an optimal algorithm for LiDAR waveform decomposition," *IEEE Geosci. Remote Sens. Lett.*, vol. 9, no. 3, pp. 482–486, May 2012.
[29] G. Zhou, S. Long, J. Xu, X. Zhou, B. Song, R. Deng, and C. Wang, "Comparison analysis of five waveform decomposition algorithms for the airborne LiDAR echo signal," *IEEE J. Sel. Topics Appl. Earth Observ. Remote Sens.*, vol. 14, pp. 7869–7880, 2021.
[30] G. Kim, J. Eom, and Y. Park, "An experiment of mutual interference between automotive LiDAR scanners," in *Proc. 12th Int. Conf. Inf. Technol.-New Generat.*, 2015, pp. 680–685.
[31] G. B. Popko, T. K. Gaylord, and C. R. Valenta, "Geometric approximation model of inter-LiDAR interference," *Opt. Eng.*, vol. 59, no. 3, Mar. 2020, Art. no. 033104.
[32] I.-P. Hwang and C.-H. Lee, "Mutual interferences of a true-random LiDAR with other LiDAR signals," *IEEE Access*, vol. 8, pp. 124123–124133, 2020.
[33] S. Grollius, A. Buchner, M. Ligges, and A. Grabmaier, "Probability of unrecognized LiDAR interference for TCSPC LiDAR," *IEEE Sensors J.*, vol. 22, no. 13, pp. 12976–12986, Jul. 2022.
[34] Y. Liang, J. Huang, M. Ren, B. Feng, X. Chen, E. Wu, G. Wu, and H. Zeng, "1550-nm time-of-flight ranging system employing laser with multiple repetition rates for reducing the range ambiguity," *Opt. Exp.*, vol. 22, no. 4, pp. 4662–4670, 1550.
[35] G. Kim and Y. Park, "LiDAR pulse coding for high resolution range imaging at improved refresh rate," *Opt. Exp.*, vol. 24, no. 21, pp. 23810–23828, 2016.
[36] T. Fersch, R. Weigel, and A. Koelpin, "A CDMA modulation technique for automotive time-of-flight LiDAR systems," *IEEE Sensors J.*, vol. 17, no. 11, pp. 3507–3516, Jun. 2017.
[37] F.-W. Lo, G.-C. Yang, W.-Y. Lin, I. Glesk, and W. C. Kwong, "2-D optical-CDMA modulation with hard-limiting for automotive time-of-flight LiDAR," *IEEE Photon. J.*, vol. 13, no. 6, pp. 1–11, Dec. 2021.
[38] G. Kim, J. Eom, and Y. Park, "Alien pulse rejection in concurrent firing LiDAR," *Remote Sens.*, vol. 14, no. 5, p. 1129, Feb. 2022.
[39] G. Lee, J. K. Park, and J. T. Kim, "OCDMA codeword switching technique to avoid interference of time-of-flight LiDAR system for autonomous vehicles," *IEEE Sensors J.*, vol. 23, no. 3, pp. 3090–3102, Feb. 2023.
[40] G. Kim, J. Eom, and Y. Park, "Concurrent transmitting LiDAR sensor with bipolar optical codes," in *Proc. Wireless Telecommun. Symp. (WTS)*, 2023, pp. 1–11.
[41] G. Kim, J. Eom, and Y. Park, "2D bipolar optical codes based concurrent transmitting LiDAR with code-inversion keying-based prime-permuted code," *IEEE Access*, vol. 11, pp. 64185–64200, 2023.
[42] *HDL-64E User Manual*, Velodyne LiDAR, San Jose, CA, USA, 2008.
[43] *GSFL-4K 3D Full Motion Video LiDAR*, Advanced Scientific Concepts LLC, Goleta, CA, USA, 2013.
[44] *S3 Solid State Sensor*, Quanergy Systems, Sunnyvale, CA, USA, 2017.
[45] H. D. Tholl, "Novel laser beam steering techniques," *Proc. SPIE*, vol. 6397, pp. 51–64, Oct. 2006.
[46] A. Li, W. Sun, W. Yi, and Q. Zuo, "Investigation of beam steering performances in rotation Risley-prism scanner," *Opt. Exp.*, vol. 24, no. 12, pp. 12840–12850, 2016.
[47] A. Li, *Double-Prism Multi-Mode Scanning: Principles and Technology*, vol. 216. Berlin, Germany: Springer, 2018.
[48] G. Garcia-Torales, "Risley prisms applications: An overview," *Proc. SPIE*, vol. 12170, pp. 136–146, May 2022.
[49] R. Ma, Q. Wang, J. Li, Y. Xia, L. Yuan, J. Yuan, J. Shi, X. Liu, Q. Tu, T. Tang, Y. Mao, Y. Huang, and G. Ren, "Robust Risley prism control based on disturbance observer for system line-of-sight stabilization," *Appl. Opt.*, vol. 61, no. 12, p. 3463, 2022.
[50] B. Ricard, "Fast Risley prisms camera steering system: Calibration and image distortions correction through the use of a three-dimensional refraction model," *Opt. Eng.*, vol. 46, no. 4, Apr. 2007, Art. no. 043201.
[51] H. Zhang, J. Cao, D. Zhou, H. Cui, Y. Cheng, and Q. Hao, "Three-dimensional computational ghost imaging using a dynamic virtual projection unit generated by Risley prisms," *Opt. Exp.*, vol. 30, no. 21, p. 39152, 2022.
[52] Z. Wang, J. Cao, Q. Hao, F. Zhang, Y. Cheng, and X. Kong, "Super-resolution imaging and field of view extension using a single camera with Risley prisms," *Rev. Sci. Instrum.*, vol. 90, no. 3, Mar. 2019.
[53] C. Gui, D. Wang, X. Huang, C. Wu, X. Chen, and H. Huang, "Super-resolution and wide-field-of-view imaging based on large-angle deflection with Risley prisms," *Sensors*, vol. 23, no. 4, p. 1793, Feb. 2023.
[54] X. Tao and H. Cho, "Variable view imaging system: An optomechatronic system for the observation of micro objects with variable view direction," *Int. J. Optomechatronics*, vol. 3, no. 2, pp. 91–115, May 2009.
[55] S.-F. Lai and C.-C. Lee, "Double-wedge prism scanner for application in thermal imaging systems," *Appl. Opt.*, vol. 57, no. 22, pp. 6290–6299, 2018.
[56] X. Tao, H. Cho, and F. Janabi-Sharifi, "Optical design of a variable view imaging system with the combination of a telecentric scanner and double wedge prisms," *Appl. Opt.*, vol. 49, no. 2, pp. 239–246, 2010.
[57] W. C. Warger II and C. A. DiMarzio, "Dual-wedge scanning confocal reflectance microscope," *Opt. Lett.*, vol. 32, no. 15, pp. 2140–2142, 2007.
[58] J. Degnan, J. McGarry, T. Zagwodzki, and T. Varghese, "Transmitter point-ahead using dual Risley prisms: Theory and experiment," in *Proc. 16th Int. Workshop Laser Ranging*, 2008, pp. 332–338.
[59] H.-M. Hoang, H. JongYoo, C. Park, J. Choi, S. H. Ahn, and J.-W. Noh, "Portable wedge prism scanner for laser surface cleaning of corroded 304L stainless steel," *Opt. Exp.*, vol. 30, no. 11, pp. 19639–19651, 2022.
[60] J. Zhou, Y. Qiao, Z. Cai, and Y. Ji, "An improved scheme for flip-OFDM based on Hartley transform in short-range IM/DD systems," *Opt. Exp.*, vol. 22, no. 17, pp. 20748–20756, 2014.
[61] K. Szczerba, P. Westbergh, J. Karout, J. S. Gustavsson, Å. Haglund, M. Karlsson, P. A. Andrekson, E. Agrell, and A. Larsson, "4-PAM for high-speed short-range optical communications," *J. Opt. Commun. Netw.*, vol. 4, no. 11, pp. 885–894, Nov. 2012.
[62] A. W. Azim, "Signal processing techniques for optical wireless communication systems," Ph.D. dissertation, Univ. Grenoble Alpes (ComUE), 2018.
[63] Z. Ghassemlooy, W. Popoola, and S. Rajbhandari, *Optical Wireless Communications: System and Channel Modelling With MATLAB*. Boca Raton, FL, USA: CRC Press, 2019.
[64] G. Kim, I. Ashraf, J. Eom, and Y. Park, "Coded pulse stream LiDAR based on optical orthogonal frequency-division multiple access," *IEEE Access*, vol. 11, pp. 142734–142747, 2023.
[65] V. Vuthea and H. Toshiyoshi, "A design of Risley scanner for LiDAR applications," in *Proc. Int. Conf. Opt. MEMS Nanophotonics (OMN)*, Jul. 2018, pp. 1–2.
[66] T. Raj, F. H. Hashim, A. B. Huddin, M. F. Ibrahim, and A. Hussain, "A survey on LiDAR scanning mechanisms," *Electronics*, vol. 9, no. 5, p. 741, Apr. 2020.
[67] X. Cao, G. Qiu, K. Wu, C. Li, and J. Chen, "LiDAR system based on lens assisted integrated beam steering," *Opt. Lett.*, vol. 45, no. 20, pp. 5816–5819, 2020.
[68] X. S. Yao, X. Liu, and P. Hao, "Scan-less 3D optical sensing/LiDAR scheme enabled by wavelength division demultiplexing and position-to-angle conversion of a lens," *Opt. Exp.*, vol. 28, no. 24, pp. 35884–35897, 2020.

[69] X. Liu, A. Li, H. Chen, J. Sun, and Z. Lu, "Scale-adaptive three-dimensional imaging using Risley-prism-based coherent LiDAR," *Opt. Lett.*, vol. 48, no. 10, pp. 2587–2590, 2023.
[70] C. Goursaud-Brugeaud, A. Julien-Vergonjanne, and J.-P. Cances, "Prime code efficiency in DS-OCDMA systems using parallel interference cancellation," *J. Commun.*, vol. 2, no. 3, pp. 51–57, May 2007.
[71] G. Kim, I. Ashraf, J. Eom, and Y. Park, "Concurrent firing light detection and ranging system for autonomous vehicles," *Remote Sens.*, vol. 13, no. 9, p. 1767, May 2021.
[72] J. Lambert, A. Carballo, A. M. Cano, P. Narksri, D. Wong, E. Takeuchi, and K. Takeda, "Performance analysis of 10 models of 3D LiDARs for automated driving," *IEEE Access*, vol. 8, pp. 131699–131722, 2020.
[73] S. Cattini, D. Cassanelli, L. D. Cecilia, L. Ferrari, and L. Rovati, "A procedure for the characterization and comparison of 3-D LiDAR systems," *IEEE Trans. Instrum. Meas.*, vol. 70, pp. 1–10, 2021.
[74] N. Muhammad and S. Lacroix, "Calibration of a rotating multi-beam LiDAR," in *Proc. IEEE/RSJ Int. Conf. Intell. Robots Syst.*, Oct. 2010, pp. 5648–5653.
[75] R. Halterman and M. Bruch, "Velodyne HDL-64E LiDAR for unmanned surface vehicle obstacle detection," *Proc. SPIE*, vol. 7692, pp. 123–130, May 2010.
[76] R. Bergelt, O. Khan, and W. Hardt, "Improving the intrinsic calibration of a Velodyne LiDAR sensor," in *Proc. IEEE SENSORS*, Oct. 2017, pp. 1–3.
[77] M. Okunsky and N. Nesterova, "Velodyne LiDAR method for sensor data decoding," *IOP Conf. Ser., Mater. Sci. Eng.*, vol. 516, no. 1, 2019, Art. no. 012018.
[78] G. Kim and Y. Park, "Independent biaxial scanning light detection and ranging system based on coded laser pulses without idle listening time," *Sensors*, vol. 18, no. 9, p. 2943, Sep. 2018.
[79] G. Kim and Y. Park, "Suitable combination of direct intensity modulation and spreading sequence for LiDAR with pulse coding," *Sensors*, vol. 18, no. 12, p. 4201, Nov. 2018.
[80] J. Eom, G. Kim, and Y. Park, "Maximizing wireless power transmission for electric vehicles with high-intensity laser power beaming and optical orthogonal frequency division multiplexing," *Transp. Res. Proc.*, vol. 70, pp. 123–129, Jan. 2023.
[81] E. E. Elsayed and B. B. Yousif, "Performance enhancement of hybrid diversity for M-ary modified pulse-position modulation and spatial modulation of MIMO-FSO systems under the atmospheric turbulence effects with geometric spreading," *Opt. Quantum Electron.*, vol. 52, no. 12, p. 508, Dec. 2020.
[82] E. E. Elsayed and B. B. Yousif, "Performance enhancement of M-ary pulse-position modulation for a wavelength division multiplexing free-space optical systems impaired by interchannel crosstalk, pointing error, and ASE noise," *Opt. Commun.*, vol. 475, Nov. 2020, Art. no. 126219.
[83] E. E. Elsayed, B. B. Yousif, and M. Singh, "Performance enhancement of hybrid fiber wavelength division multiplexing passive optical network FSO systems using M-ary DPPM techniques under interchannel crosstalk and atmospheric turbulence," *Opt. Quantum Electron.*, vol. 54, no. 2, p. 116, Feb. 2022.
[84] M. R. Hayal, E. E. Elsayed, D. Kakati, M. Singh, A. Elfikky, A. I. Boghdady, A. Grover, S. Mehta, S. A. H. Mohsan, and I. Nurhidayat, "Modeling and investigation on the performance enhancement of hovering UAV-based FSO relay optical wireless communication systems under pointing errors and atmospheric turbulence effects," *Opt. Quantum Electron.*, vol. 55, no. 7, p. 625, Jul. 2023.
[85] S. Li, J. Cao, Y. Cheng, L. Meng, W. Xia, Q. Hao, and Y. Fang, "Spatially adaptive retina-like sampling method for imaging LiDAR," *IEEE Photon. J.*, vol. 11, no. 3, pp. 1–16, Jun. 2019.
[86] Y. Cao, C. Xiao, B. Cyr, Y. Zhou, W. Park, S. Rampazzi, Q. A. Chen, K. Fu, and Z. M. Mao, "Adversarial sensor attack on LiDAR-based perception in autonomous driving," in *Proc. ACM SIGSAC Conf. Comput. Commun. Secur.*, Nov. 2019, pp. 2267–2281.
[87] R. Heinzler, P. Schindler, J. Seekircher, W. Ritter, and W. Stork, "Weather influence and classification with automotive LiDAR sensors," in *Proc. IEEE Intell. Vehicles Symp. (IV)*, Jun. 2019, pp. 1527–1534.
[88] A. M. Wallace, A. Halimi, and G. S. Buller, "Full waveform LiDAR for adverse weather conditions," *IEEE Trans. Veh. Technol.*, vol. 69, no. 7, pp. 7064–7077, Jul. 2020.
[89] D. Smith, Q. Abdullah, D. Maune, and H. Heidemann, "New ASPRS positional accuracy standards for digital geospatial data released," *Photogramm. Eng. Remote Sens.*, vol. 81, pp. 1073–1085, Jan. 2015.
[90] M. T. Sullivan, "Synopsis of Risley prism beam pointer," Lockheed Martin Space Syst. Hanover Street, Palo Alto, CA, USA, Tech. Rep., 3251, 2006.

GUNZUNG KIM (Member, IEEE) was born in Daegu, Republic of Korea, in 1972. He received the B.S. and M.S. degrees in computer engineering and the Ph.D. degree in multimedia and communication engineering from Yeungnam University, Republic of Korea, in 1995, 1997, and 2019, respectively. He is currently a Research Professor with Yeungnam University. His research interests include LiDAR, optical communication, and vehicle software.

IMRAN ASHRAF received the M.S. degree in computer science from the Blekinge Institute of Technology, Karlskrona, Sweden, in 2010, and the Ph.D. degree in information and communication engineering from Yeungnam University, Gyeongsan-si, South Korea, in 2018. He was a Postdoctoral Fellow with Yeungnam University, where he is currently an Assistant Professor with the Department of Information and Communication Engineering. His research interests include indoor positioning and localization, indoor location-based services in wireless communication, smart sensors (LiDAR) for smart cars, and data mining.

JEONGSOOK EOM was born in Daegu, Republic of Korea, in 1975. She received the B.S. and M.S. degrees in computer engineering from Yeungnam University, Republic of Korea, in 1998 and 2001, respectively, where she is currently pursuing the Ph.D. degree in multimedia and communication engineering. Her research interests include LiDAR, optical communication, and mutual interference between active sensors.

YONGWAN PARK (Member, IEEE) was born in Daegu, Republic of Korea, in 1959. He received the B.E. and M.E. degrees in electrical engineering from Kyungpook University, Daegu, Republic of Korea, in 1982 and 1984, respectively, and the M.S. and Ph.D. degrees in electrical engineering from the State University of New York at Buffalo, USA, in 1989 and 1992, respectively. He is currently a Professor with Yeungnam University and the Chairman of the 5G Forum Convergence Service Committee, Republic of Korea. His research interests include 5G systems in communication, OFDM, PAPR reduction, and indoor location-based services in wireless communication and smart sensors (LiDAR) for smart cars.